Supporting Information

Homo- and heterometallic chiral dynamic architectures from allyl-palladium(II) building blocks

Montserrat Ferrer,[a,b*] Albert Gallen,[a*] Manuel Martínez,[a,b] Mercè Rocamora,[a] Rakesh Puttreddy[c] and Kari Rissanen[c]

[a] Departament de Química Inorgànica i Orgànica, Secció de Química Inorgànica, Universitat de Barcelona, Martí i Franquès, 1-11, E-08028, Barcelona, Spain.

[b] Institut de Nanociència i Nanotecnologia (IN^{2}UB). Universitat de Barcelona, 08028 Barcelona, Spain

[c] Department of Chemistry, University of Jyväskylä, POB 35, 40014 Jyväskylä, Finland.

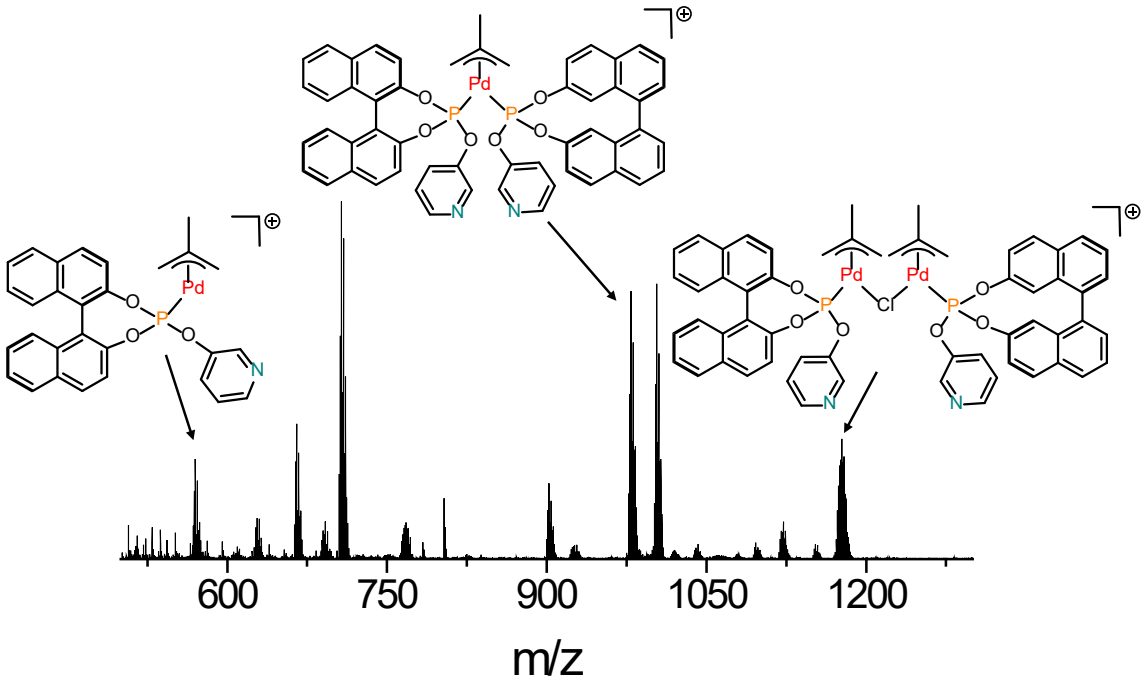

Figure S1. ESI(+)-HRMS spectrum of **[PdCl(η^3-2-Me-C$_3$H$_4$){(*S*)-BINOL-3-POpy}]**.

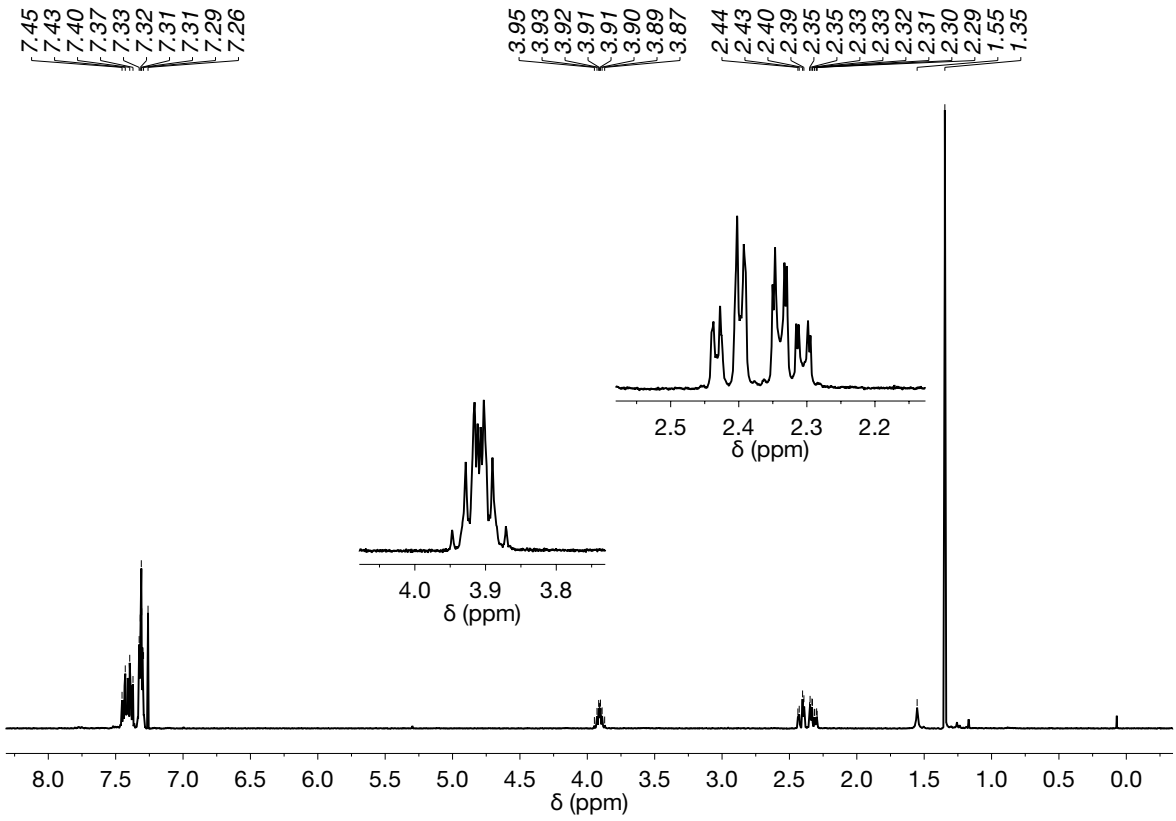

Figure S2. ^{1}H NMR of **(*S*,*S*)-DIOP** in $CDCl_3$ at 298 K.

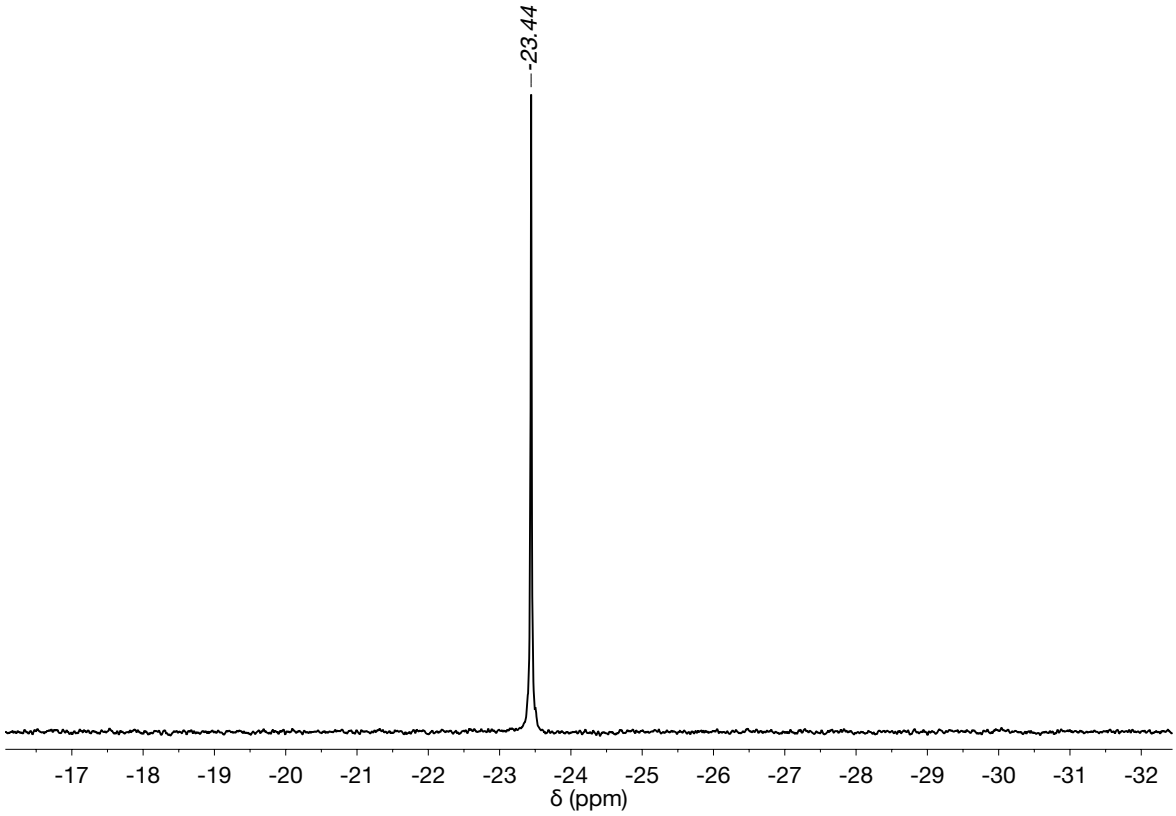

Figure S3. $^{31}P\{^{1}H\}$ NMR of **(*S,S*)-DIOP** in $CDCl_3$ at 298 K.

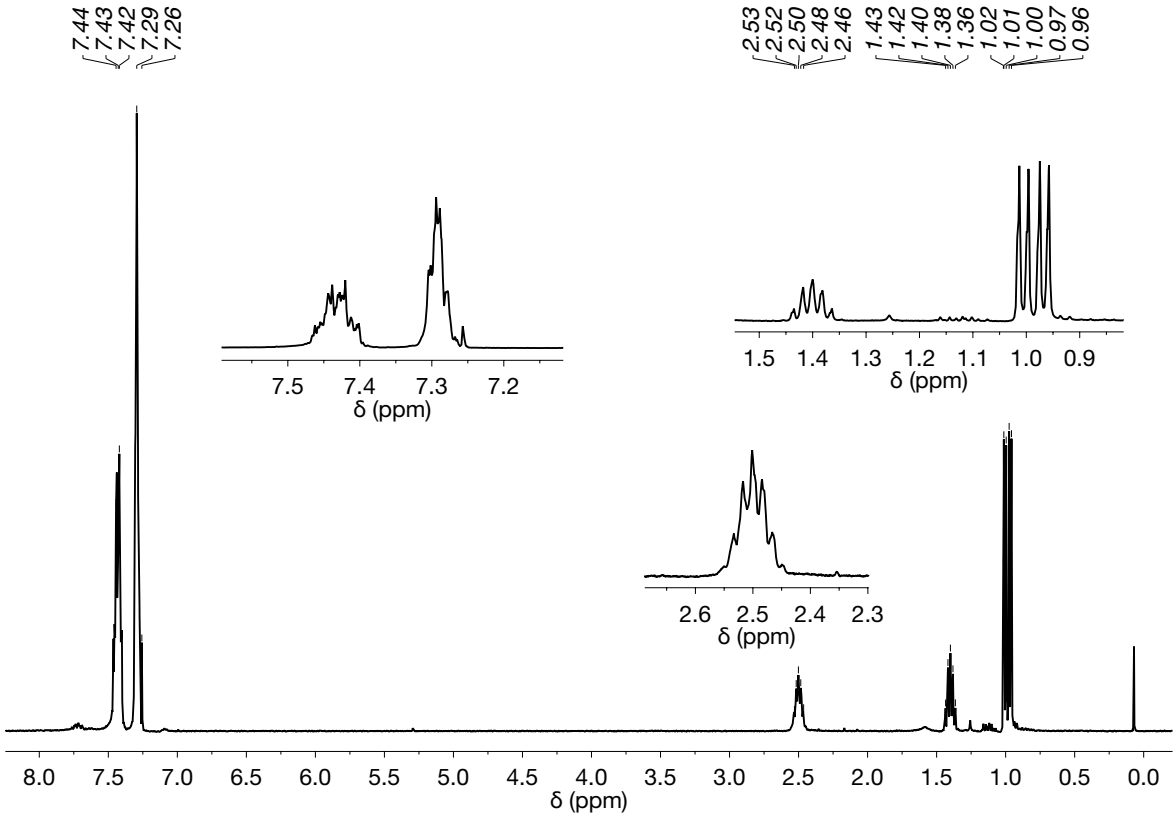

Figure S4. ^{1}H NMR of **(*S,S*)-BDPP** in $CDCl_3$ at 298 K.

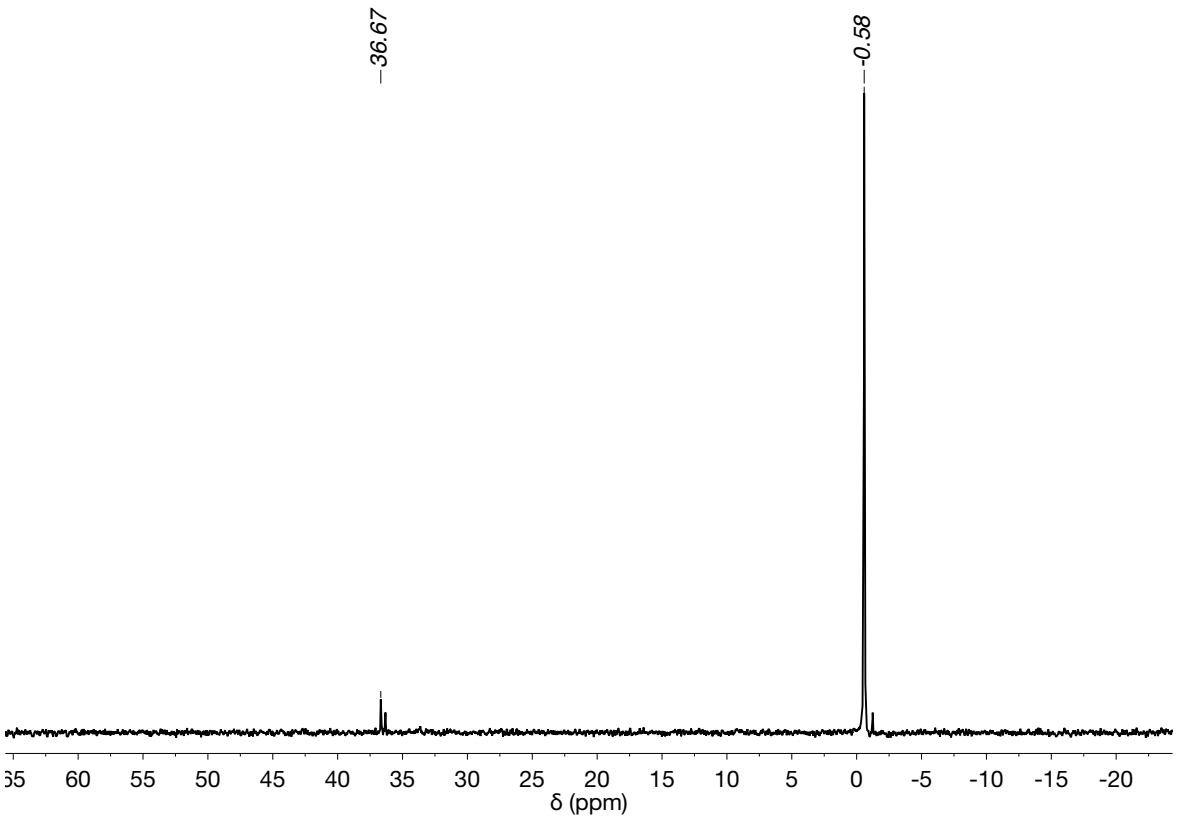

Figure S5. $^{31}P\{^{1}H\}$ NMR of **(*S,S*)-DIOP** in $CDCl_3$ at 298 K.

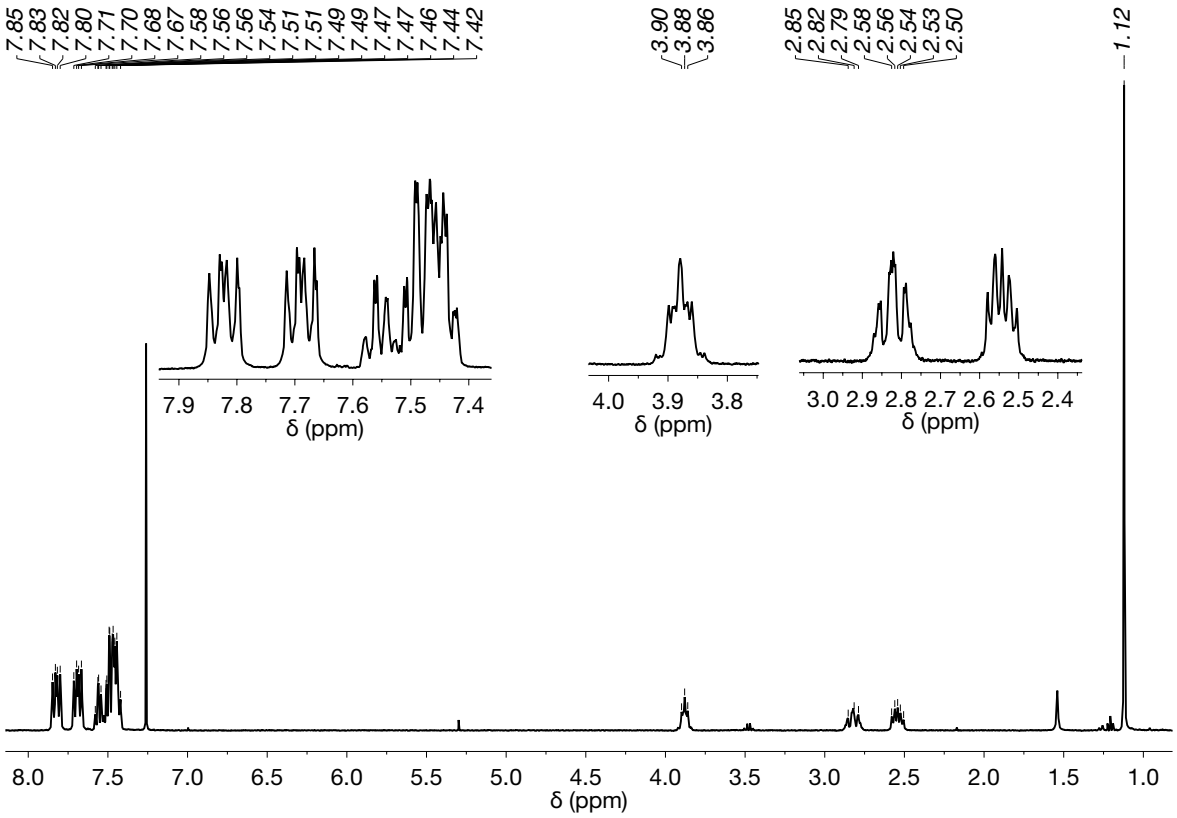

Figure S6. ^{1}H NMR of **[$PdCl_2$((*S,S*)DIOP)]** in $CDCl_3$ at 298 K.

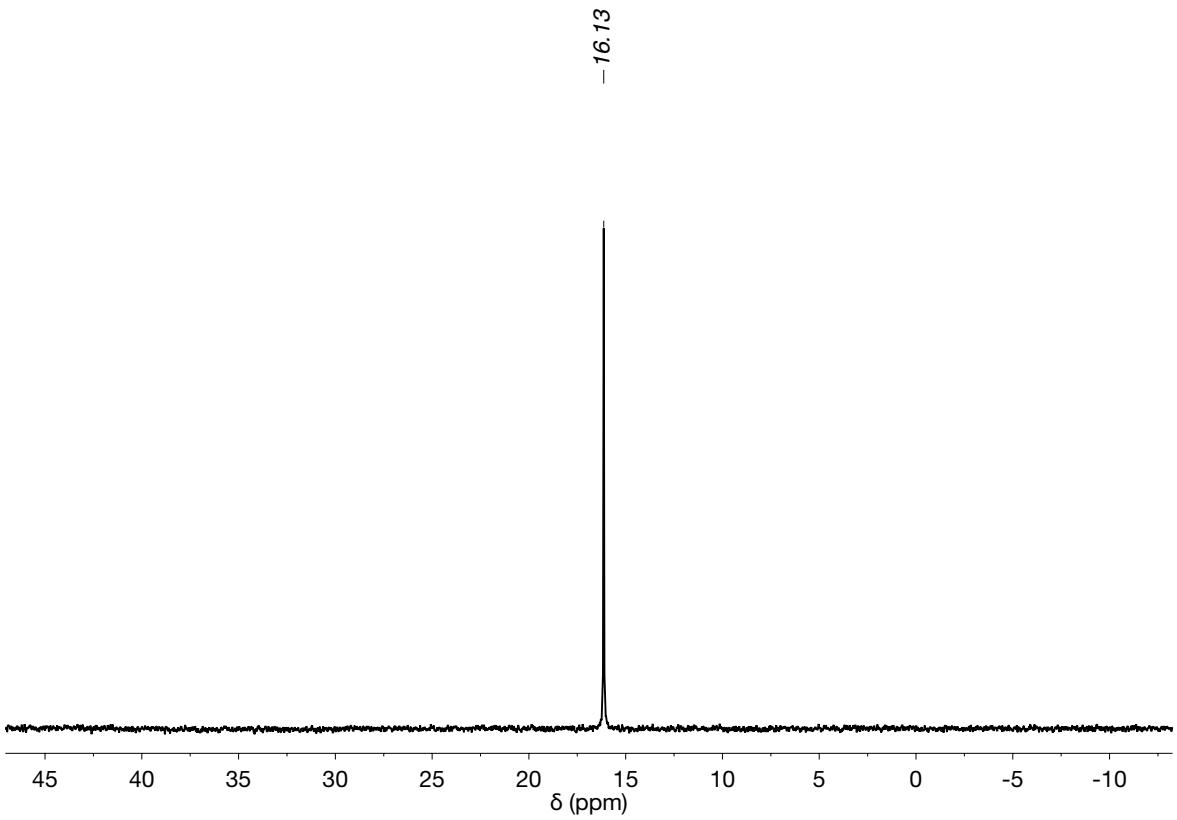

Figure S7. $^{31}P\{^{1}H\}$ NMR of **[PdCl$_2$((*S,S*)DIOP)]** in $CDCl_3$ at 298 K.

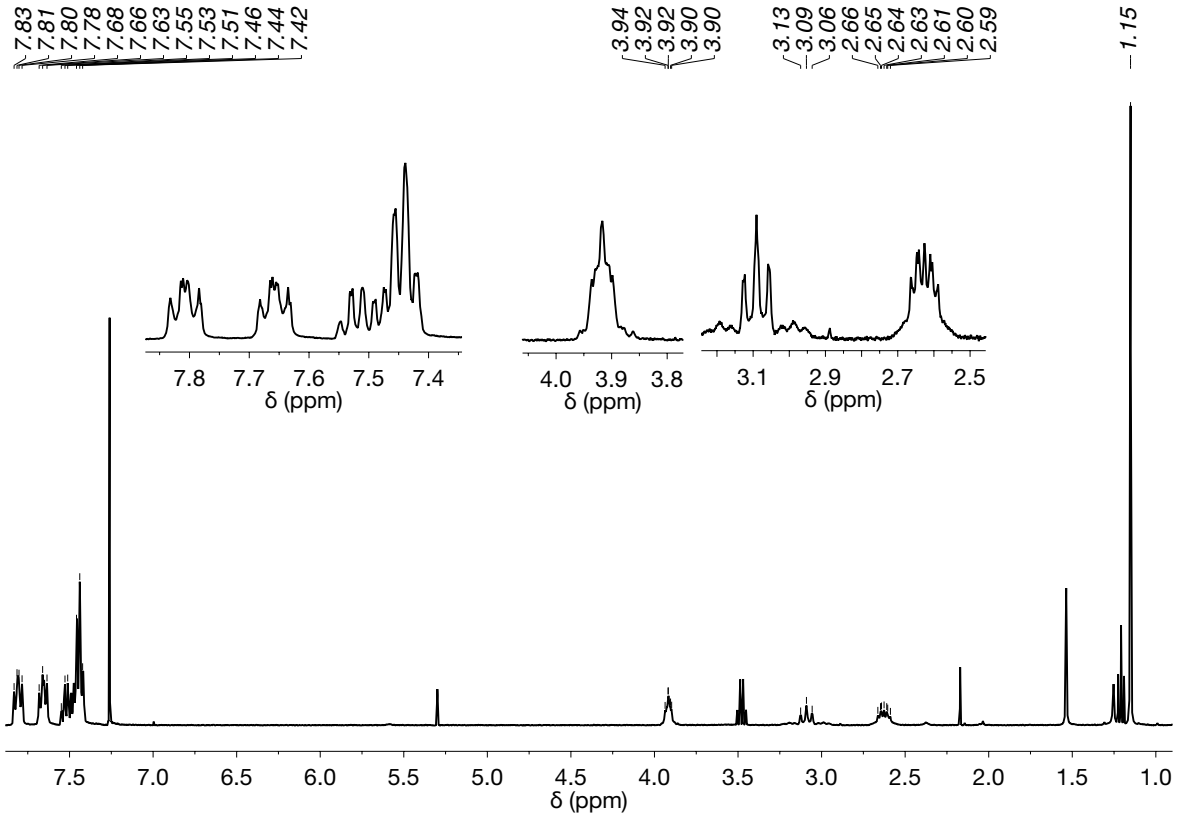

Figure S8. ^{1}H NMR of **[PtCl$_2$((*S,S*)DIOP)]** in $CDCl_3$ at 298 K.

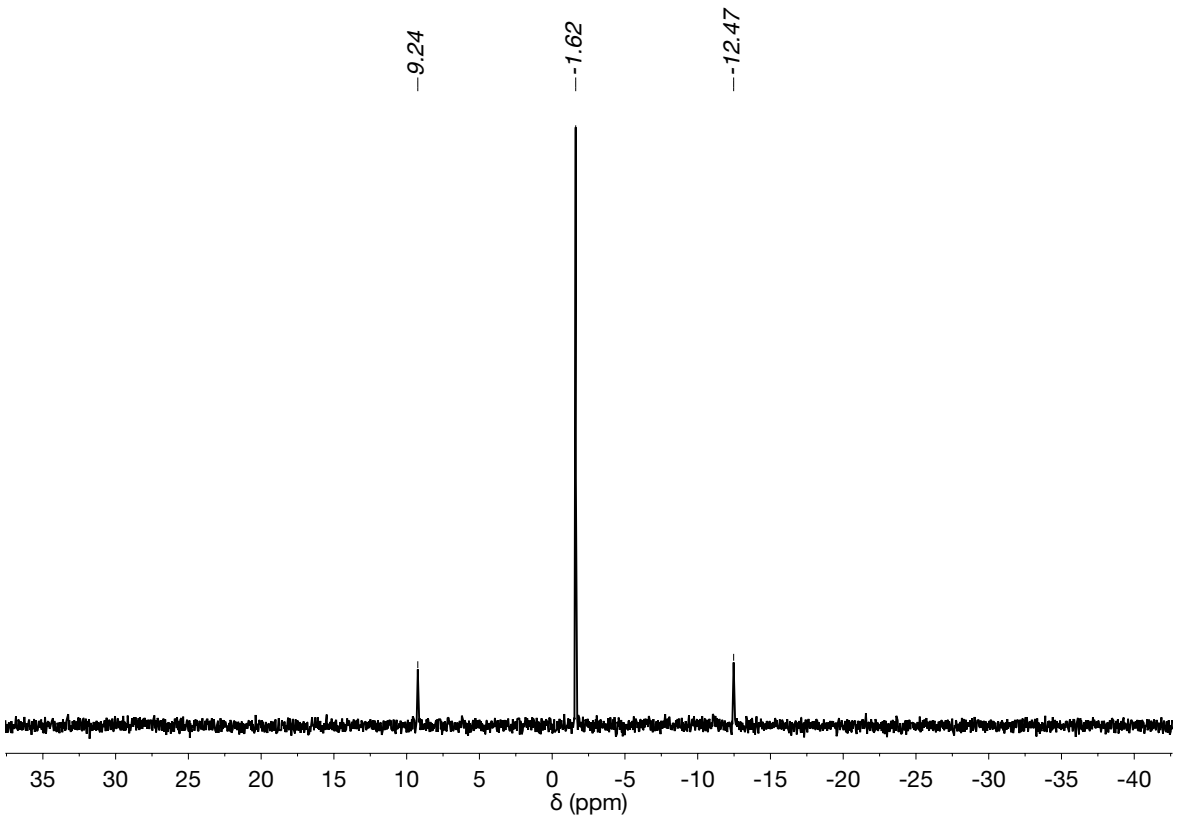

Figure S9. $^{31}P\{^{1}H\}$ NMR of **[PtCl$_2$((*S,S*)DIOP)]** in $CDCl_3$ at 298 K.

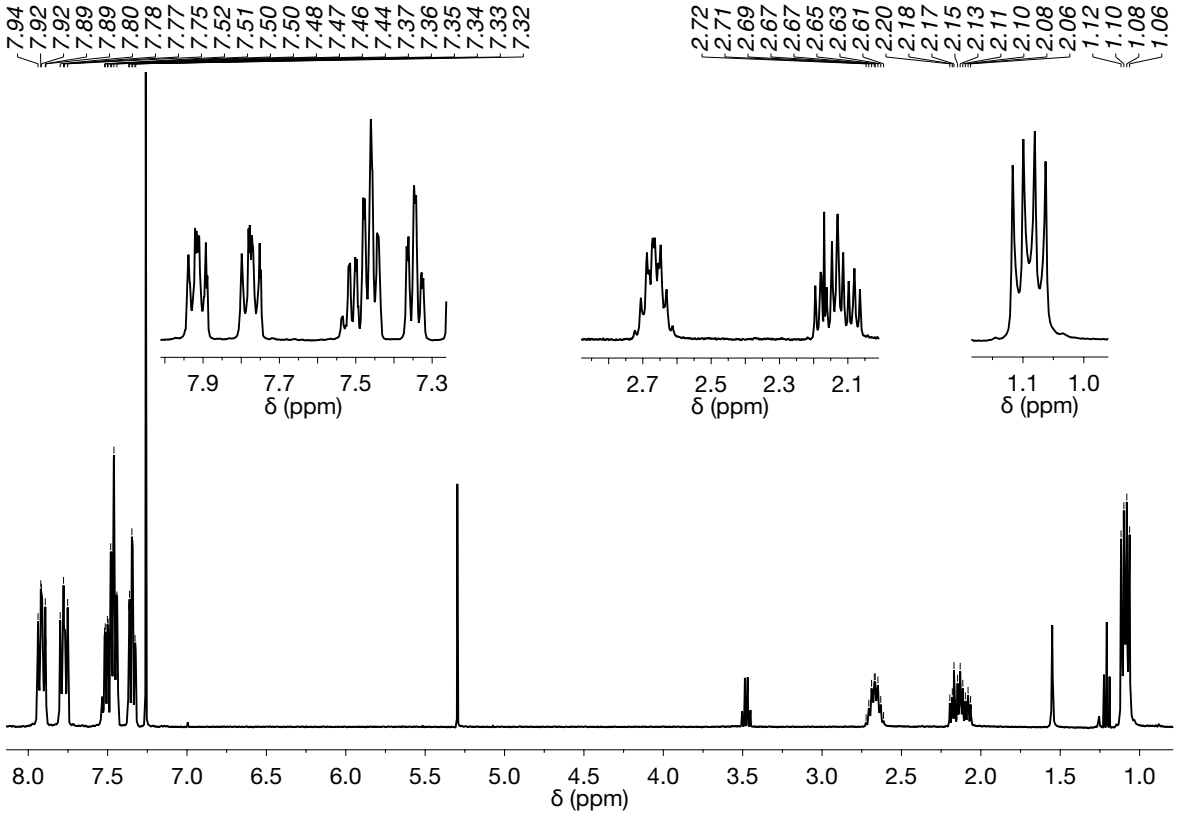

Figure S10. ^{1}H NMR of **[PdCl$_2$((*S,S*)BDPP)]** in $CDCl_3$ at 298 K.

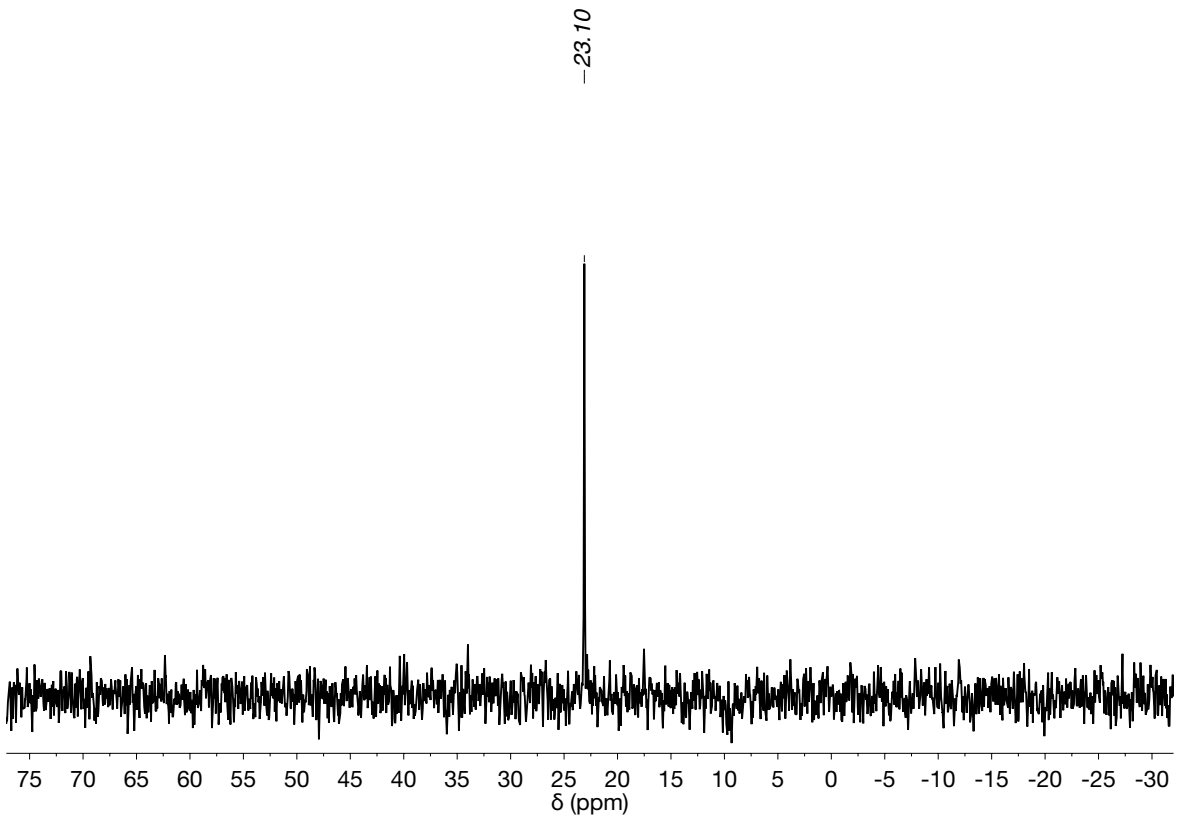

Figure S11. $^{31}P\{^{1}H\}$ NMR of **[$PdCl_2$((*S,S*)BDPP)]** in $CDCl_3$ at 298 K.

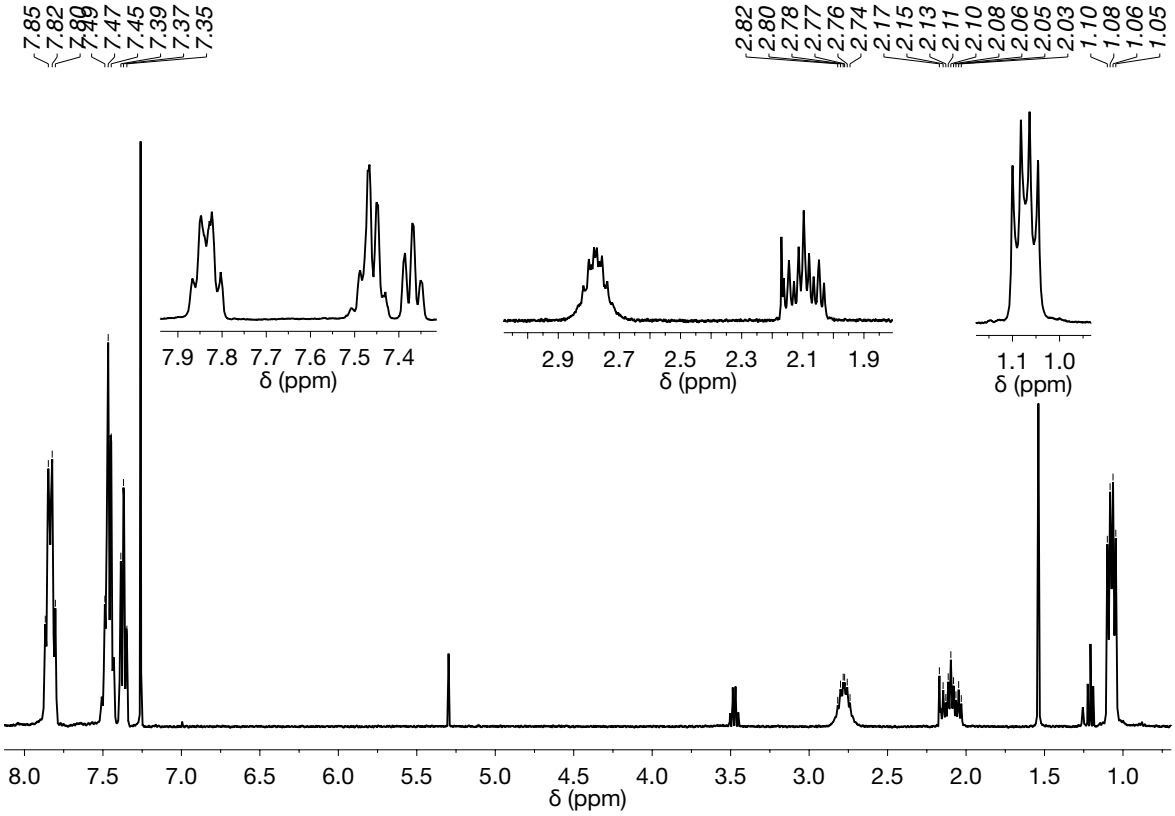

Figure S12. ^{1}H NMR of **[$PtCl_2$((*S,S*)BDPP)]** in $CDCl_3$ at 298 K.

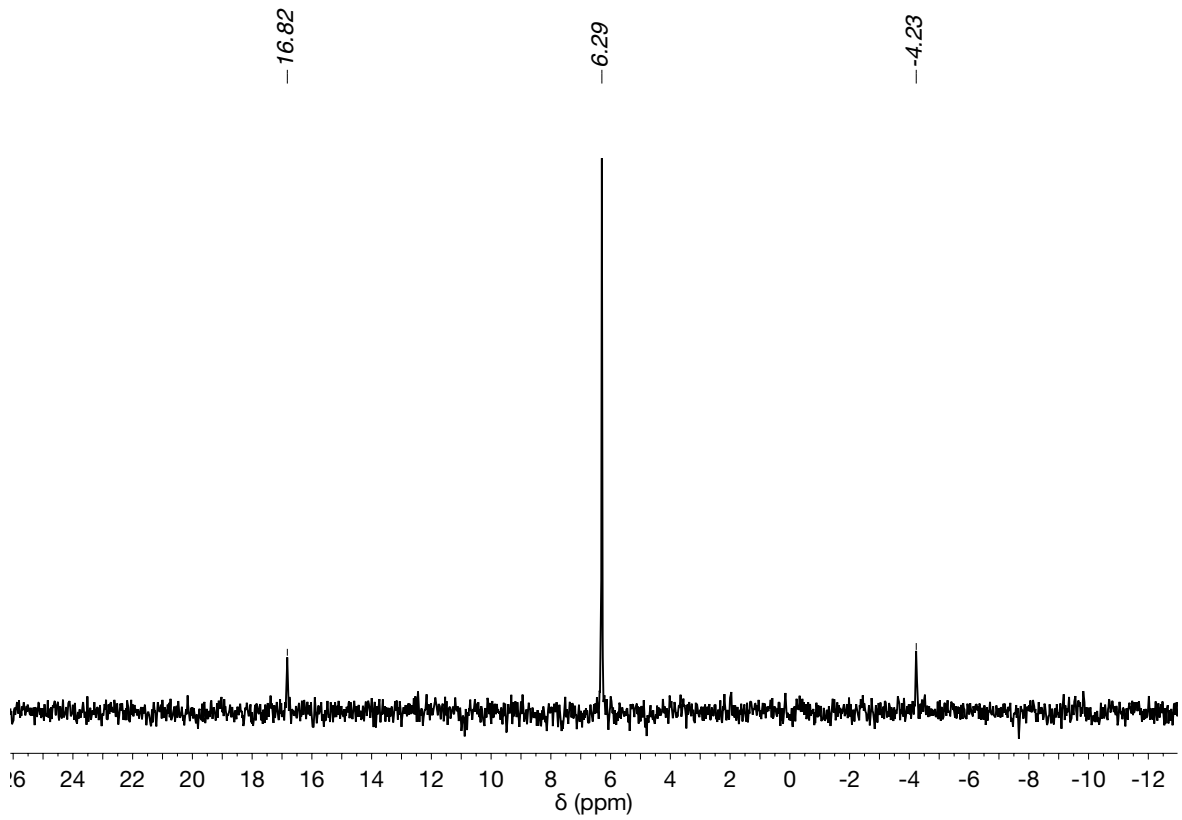

Figure S13. $^{31}P\{^{1}H\}$ NMR of **[PtCl$_2$((*S,S*)BDPP)]** in $CDCl_3$ at 298 K.

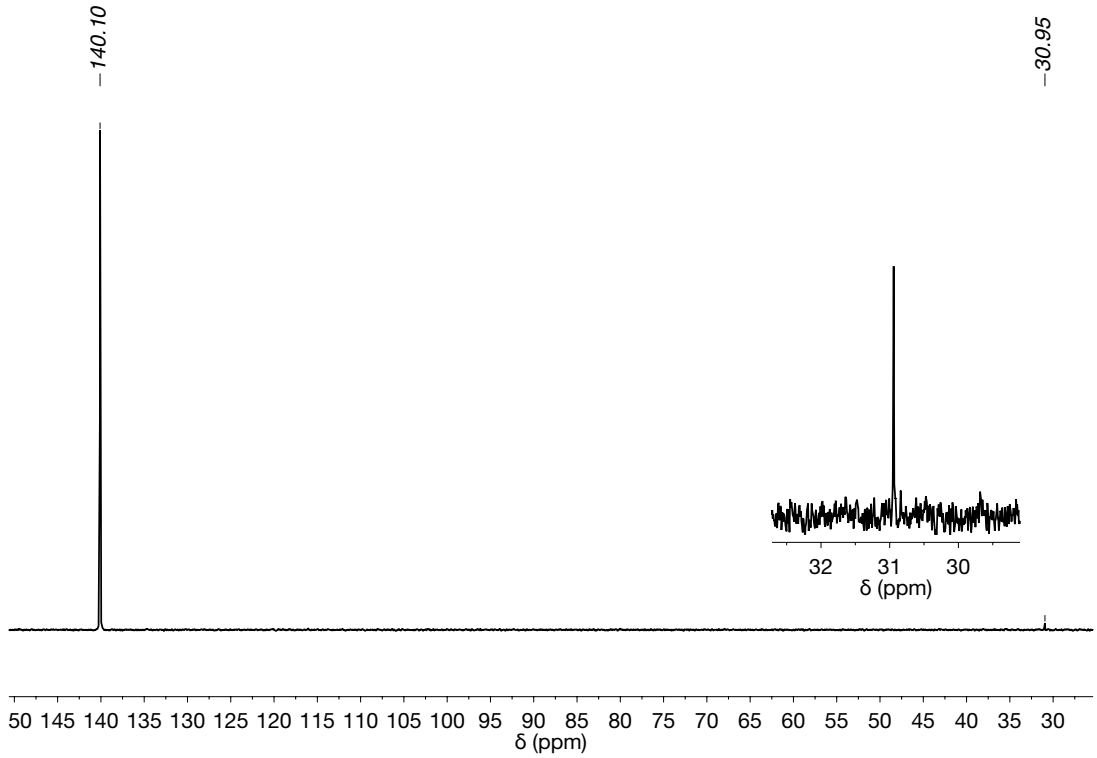

Figure S14. INSET $^{31}P\{^{1}H\}$ NMR of **[Pd((*S,S*)DIOP)(H$_2$O)$_2$](CF$_3$SO$_3$)$_2$** (**1Pd**) in CH_2Cl_2 solution at 298 K (signal at 140.1 ppm belongs to $P(OMe)_3$ used as external reference).

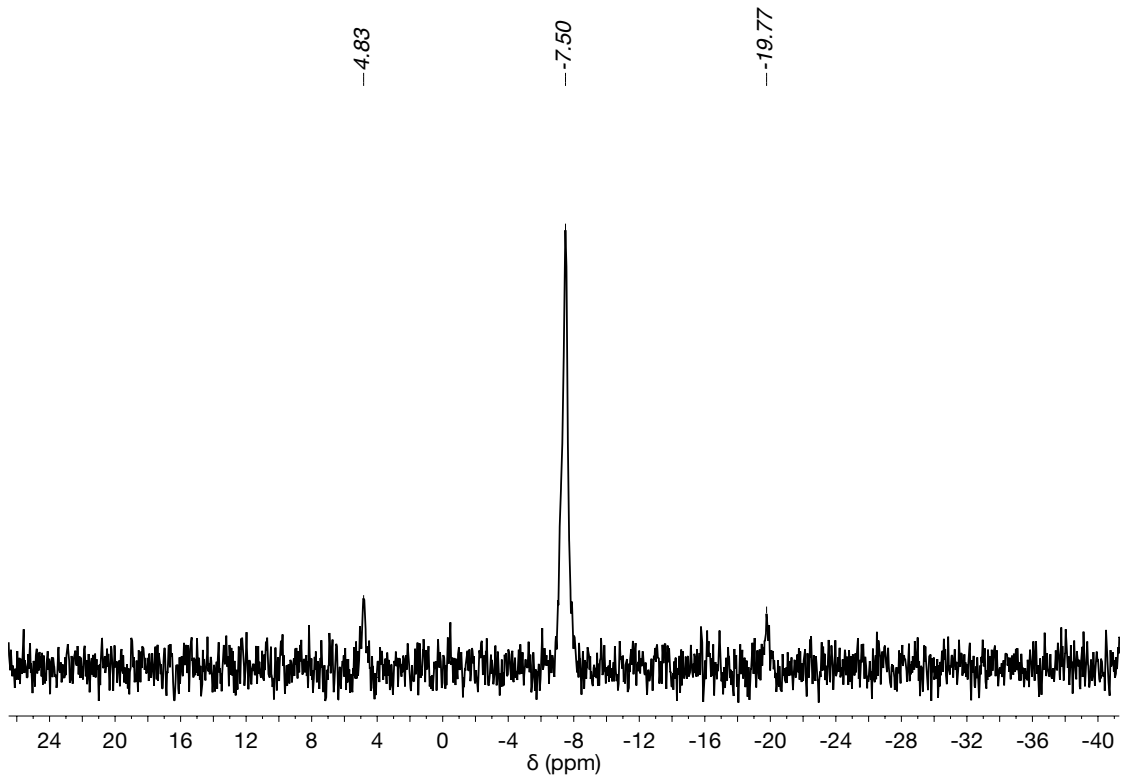

Figure S15. INSET $^{31}P\{^{1}H\}$ NMR of **[Pt((S,S)DIOP)(H_2O)$_2$](CF_3SO_3)$_2$** (**1Pt**) in CH_2Cl_2 solution at 298 K.

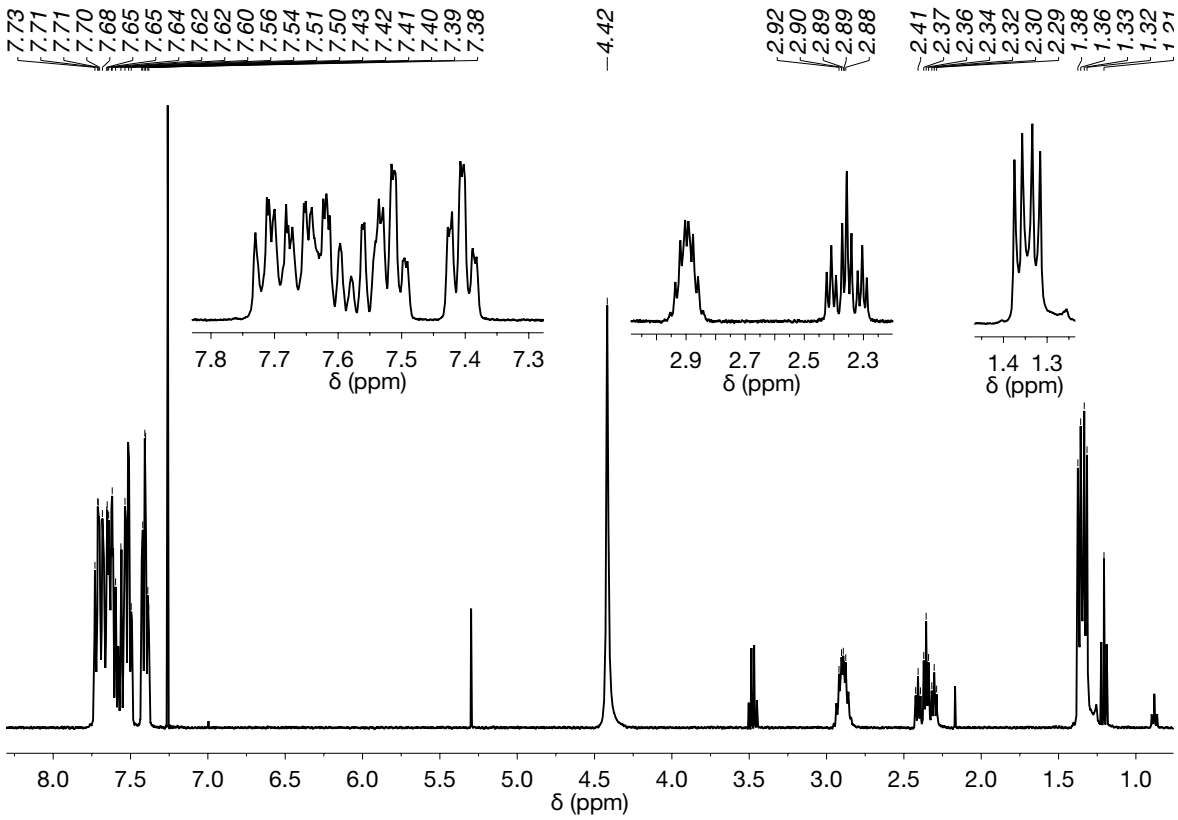

Figure S16. ^{1}H NMR of **[Pd((*S,S*)BDPP)(H_2O)$_2$](CF_3SO_3)$_2$** (**2Pd**) in $CDCl_3$ at 298 K.

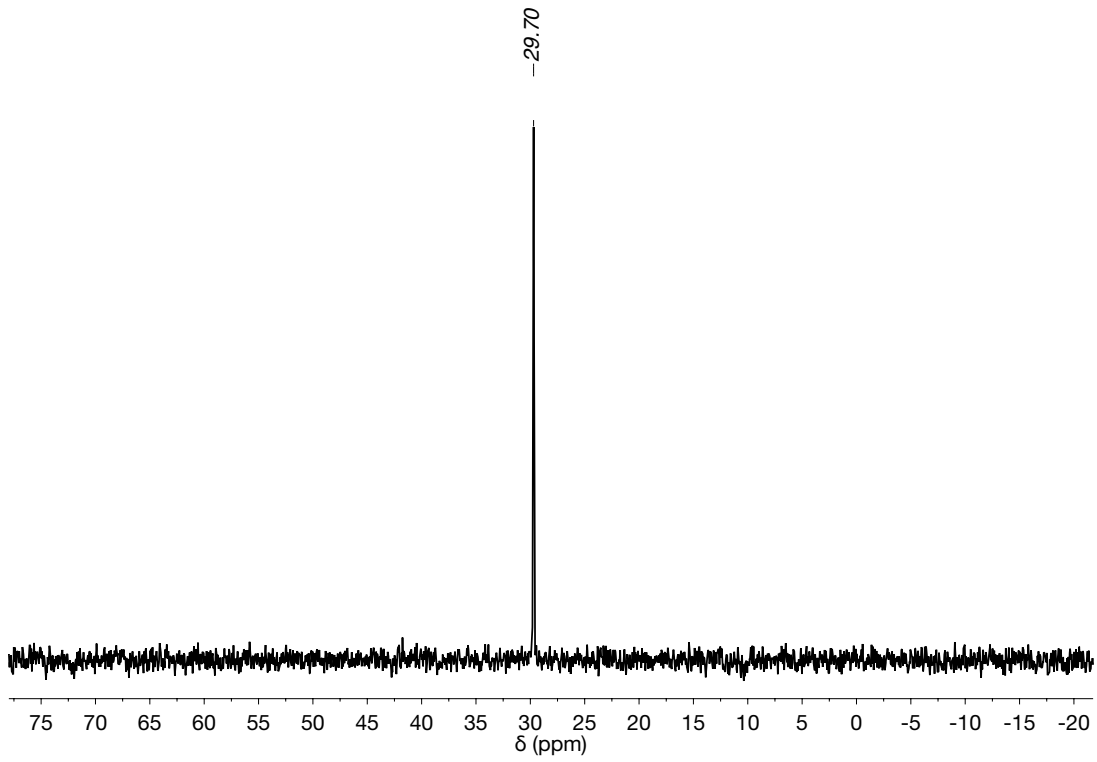

Figure S17. $^{31}P\{^{1}H\}$ NMR of **[Pd((*S,S*)BDPP)(H_2O)$_2$](CF_3SO_3)$_2$** (**2Pd**) in $CDCl_3$ at 298 K.

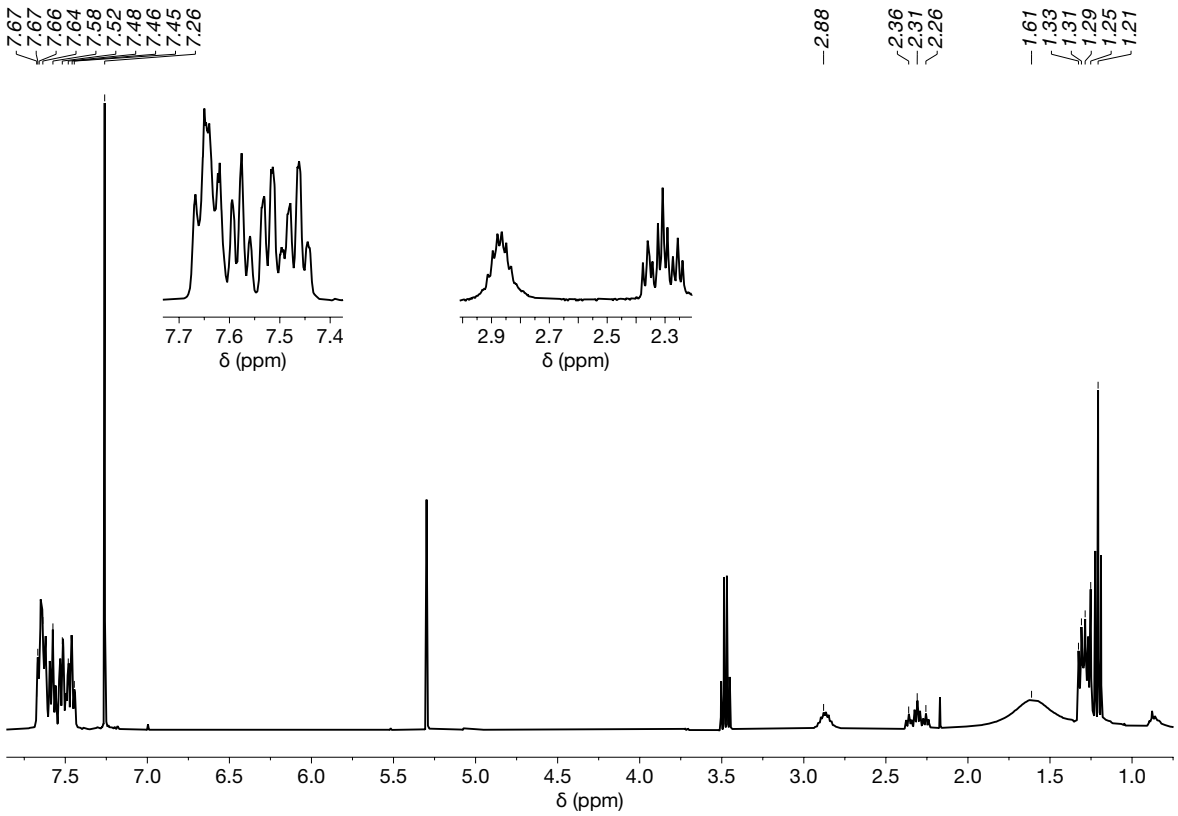

Figure S18. ^{1}H NMR of **[Pt((*S,S*)BDPP)(H_2O)$_2$](CF_3SO_3)$_2$** (**2Pt**) in $CDCl_3$ at 298 K.

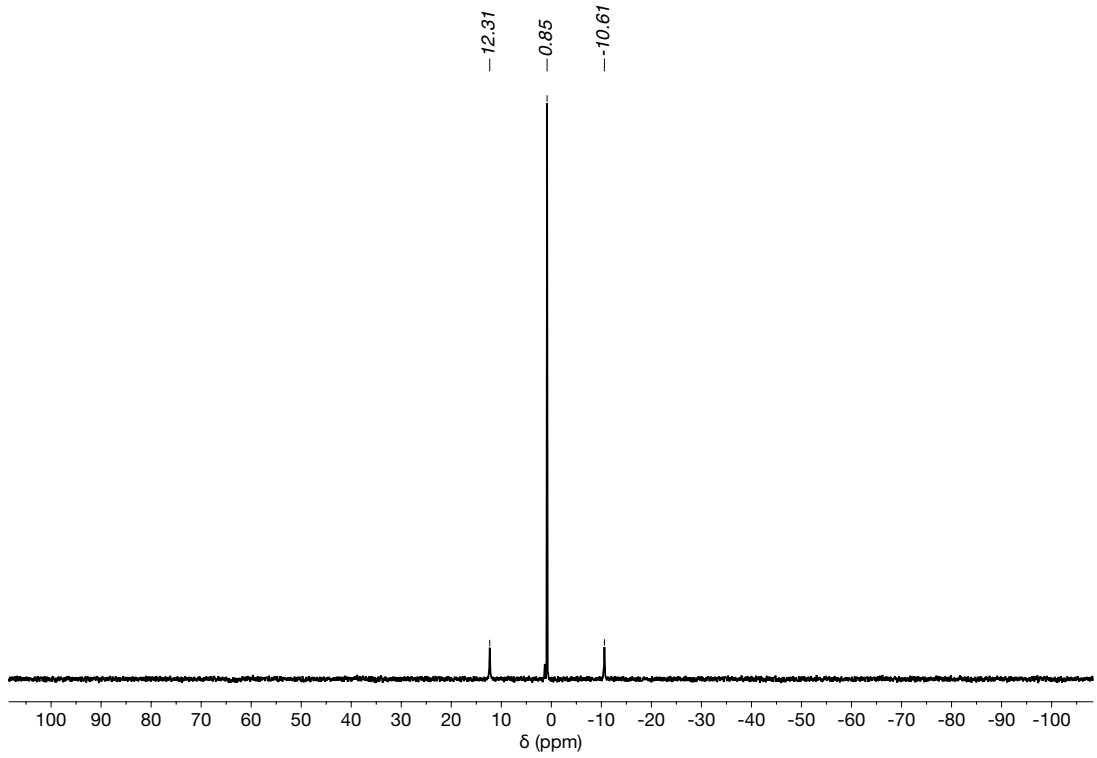

Figure S19. $^{31}P\{^{1}H\}$ NMR of **[Pt((*S,S*)BDPP)(H$_2$O)$_2$](CF$_3$SO$_3$)$_2$** (**2Pt**) in $CDCl_3$ at 298 K.

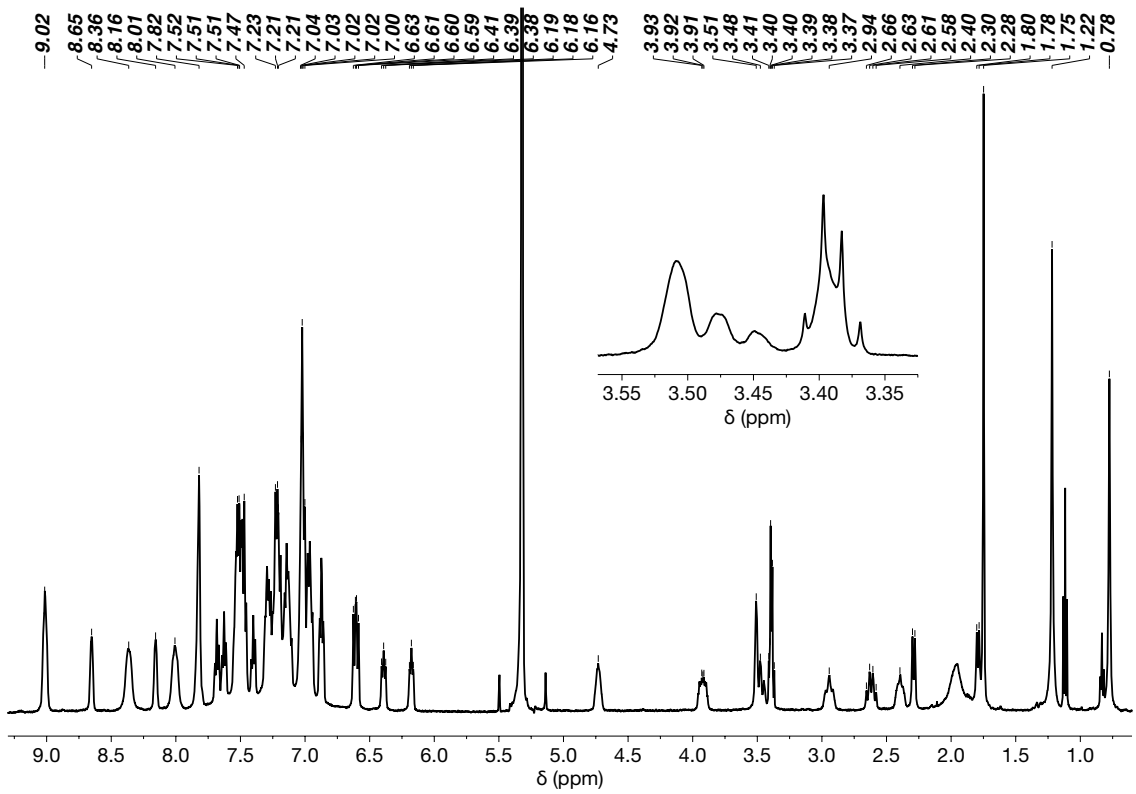

Figure S20. ^{1}H NMR of **[{Pd(η^3-2-Me-C$_3$H$_4$)}$_2$(4-PPh$_2$py)$_4${Pd(DIOP)}$_2$](CF$_3$SO$_3$)$_6$** (**[1PdaL]$_2$**) in CD_2Cl_2 at 238 K.

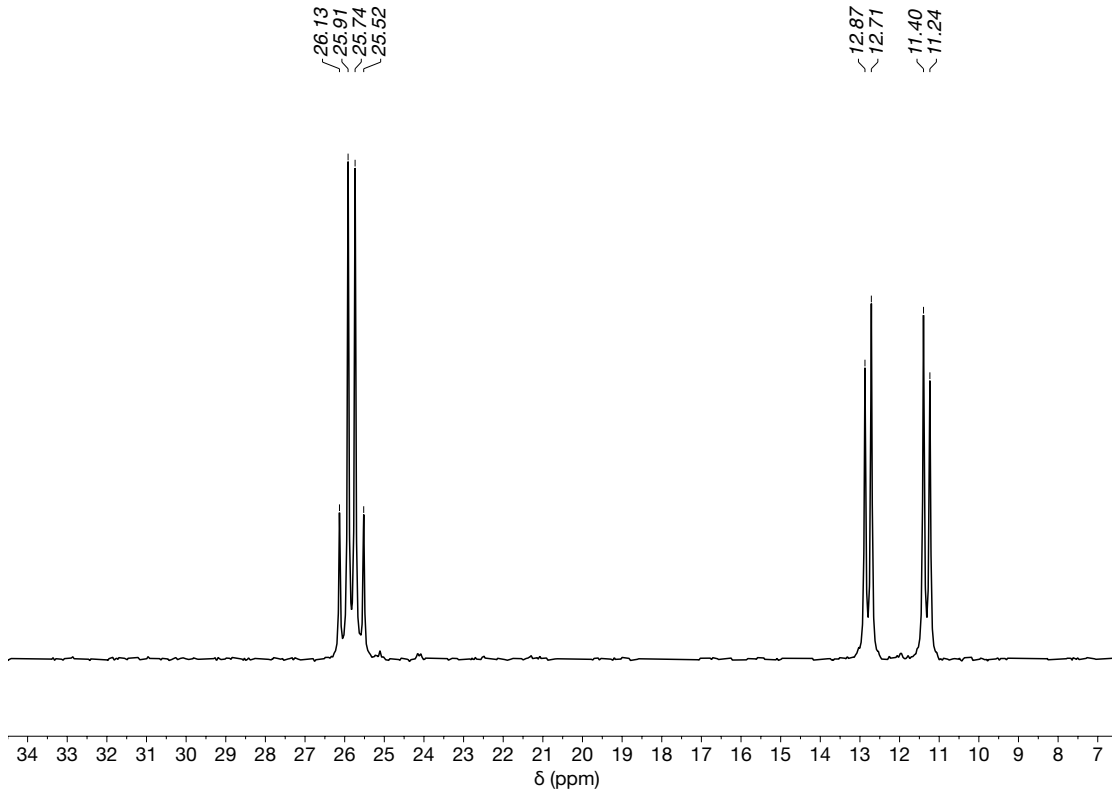

Figure S21. $^{31}P\{^{1}H\}$ NMR of **[{Pd(η^3-2-Me-C$_3$H$_4$)}$_2$(4-PPh$_2$py)$_4${Pd(DIOP)}$_2$](CF$_3$SO$_3$)$_6$ ([1PdaL]$_2$)** in $CDCl_3$ at 298 K.

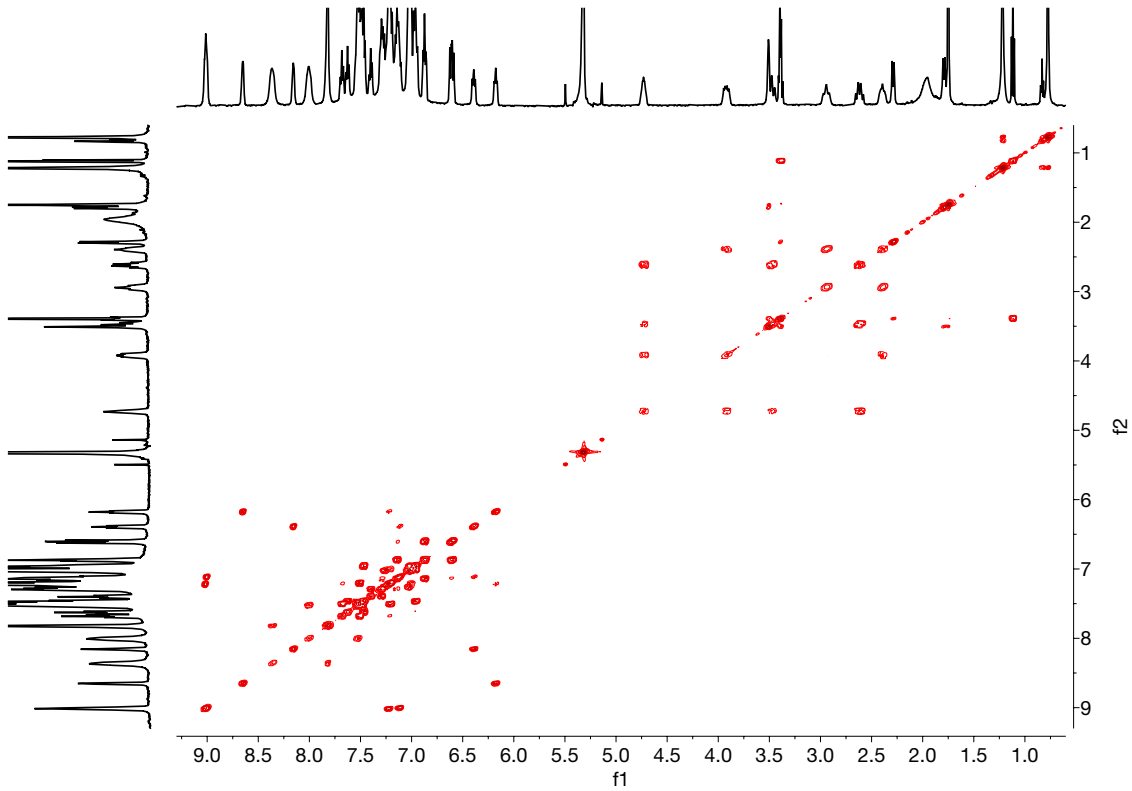

Figure S22. ^{1}H-^{1}H COSY NMR of **[{Pd(η^3-2-Me-C$_3$H$_4$)}$_2$(4-PPh$_2$py)$_4${Pd(DIOP)}$_2$](CF$_3$SO$_3$)$_6$ ([1PdaL]$_2$)** in CD_2Cl_2 at 238 K.

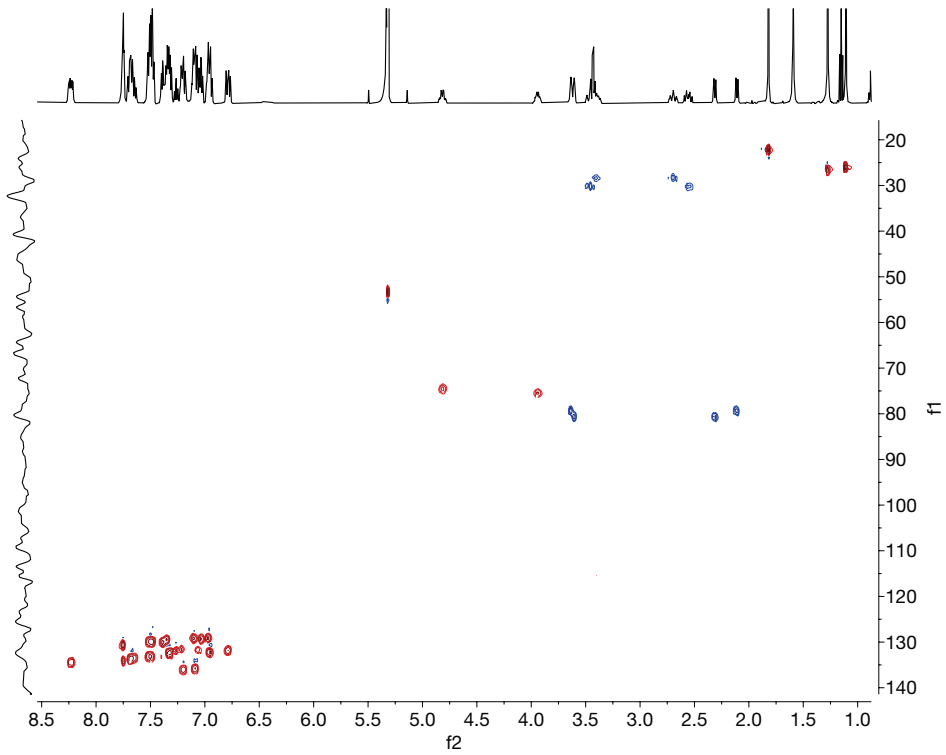

Figure S23. ^{1}H-^{13}C gHSQC NMR of **[{Pd(η^{3}-2-Me-C$_{3}$H$_{4}$)}$_{2}$(4-PPh$_{2}$py)$_{4}$\{Pd(DIOP)\}$_{2}$](CF$_{3}$SO$_{3}$)$_{6}$ ([1PdaL]$_{2}$)** in CD_2Cl_2 at 298 K.

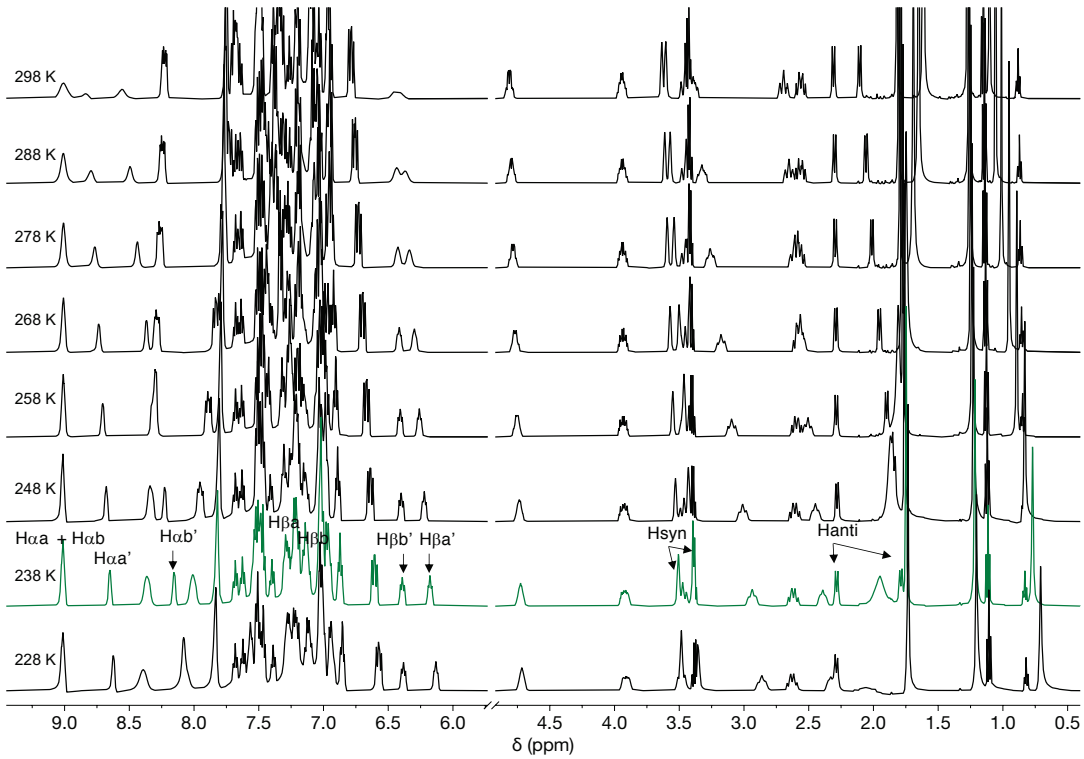

Figure S24. Variable temperature ^{1}H NMR spectra of **[{Pd(η^{3}-2-Me-C$_{3}$H$_{4}$)}$_{2}$(4-PPh$_{2}$py)$_{4}$\{Pd(DIOP)\}$_{2}$](CF$_{3}$SO$_{3}$)$_{6}$ ([1PdaL]$_{2}$)** in CD_2Cl_2

.

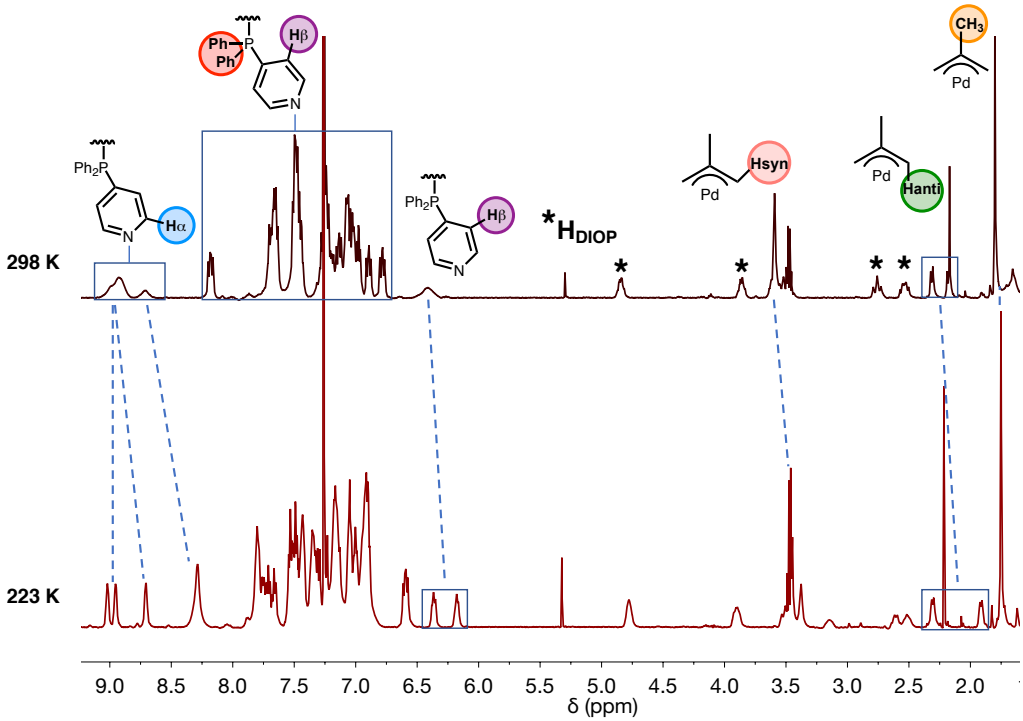

Figure S25. Comparative of the ^{1}H NMR spectra of **[{Pd(η^3-2-Me-C$_3$H$_4$)}$_2$(4-PPh$_2$py)$_4${Pd(DIOP)}$_2$](CF$_3$SO$_3$)$_6$ ([1PdaL]$_2$)** in CDCl$_3$ at 298 K (top) and 223 K (bottom).

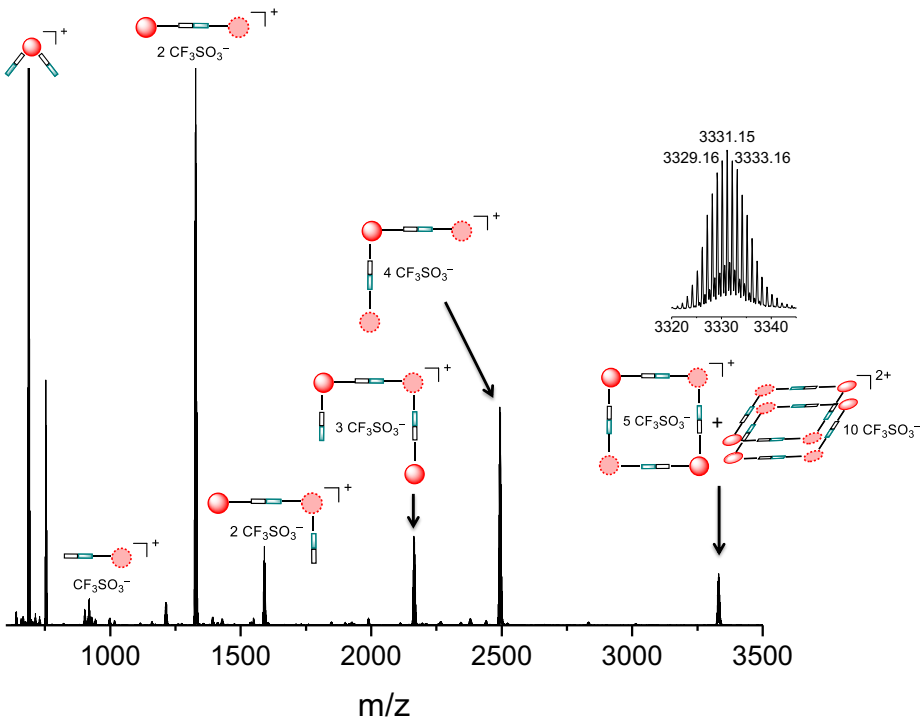

Figure S26. ESI(+)-HRMS spectrum of **[{Pd(η^3-2-Me-C$_3$H$_4$)}$_2$(4-PPh$_2$py)$_4${Pd(DIOP)}$_2$](CF$_3$SO$_3$)$_6$ ([1PdaL]$_2$)**.

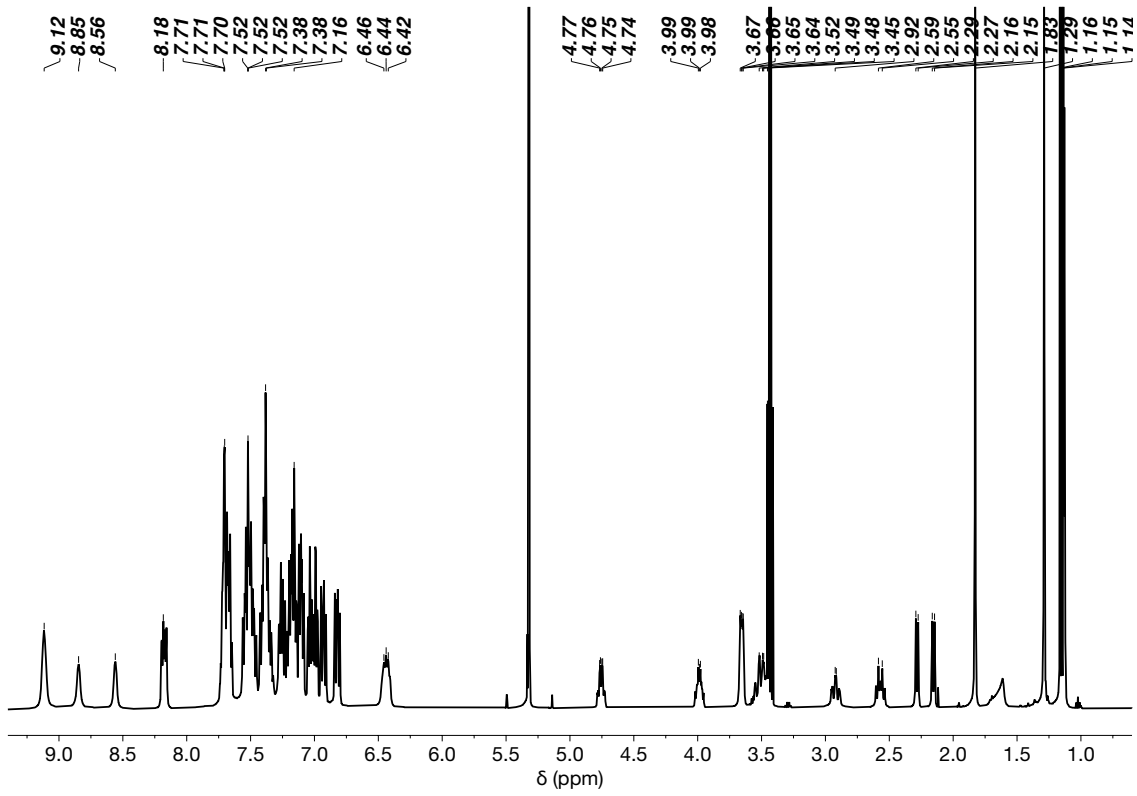

Figure S27. ^{1}H NMR of **[{Pd(η^3-2-Me-C$_3$H$_4$)}$_2$(4-PPh$_2$py)$_4${Pt(DIOP)}$_2$](CF$_3$SO$_3$)$_6$** (**[1PtaL]$_2$**) in CD_2Cl_2 at 298 K.

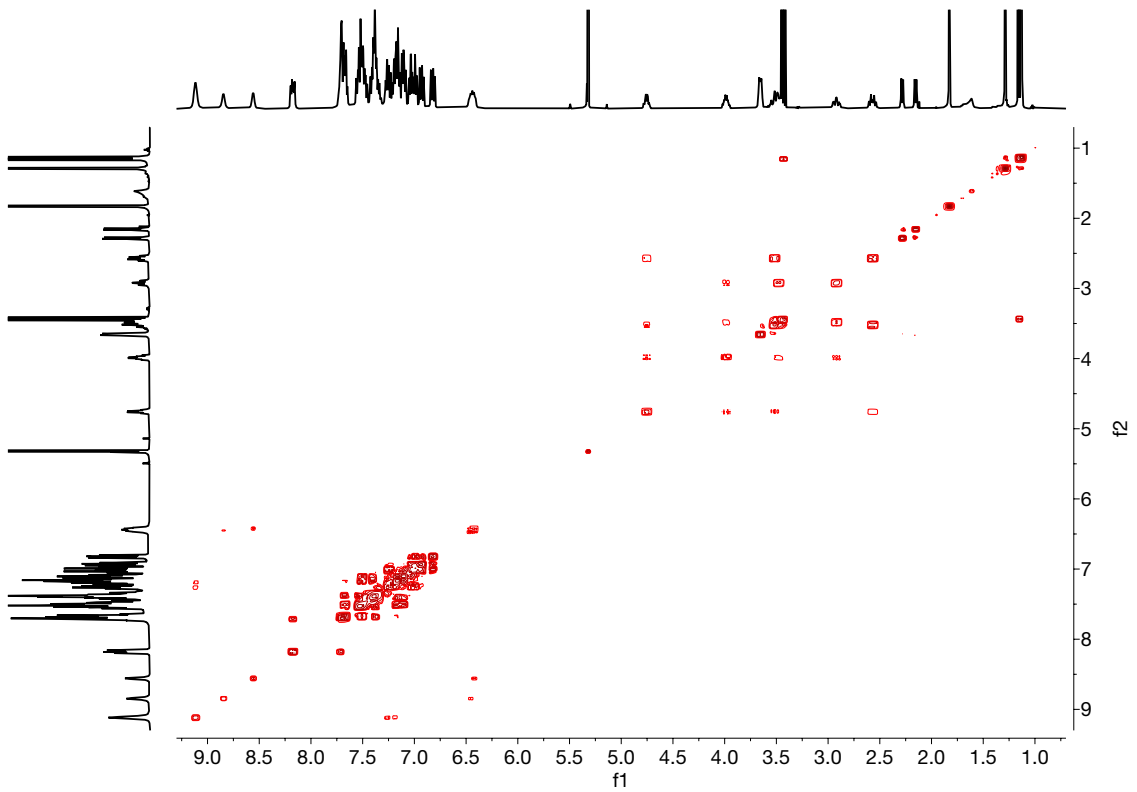

Figure S28.^{1}H-^{1}H COSY NMR of **[{Pd(η^3-2-Me-C$_3$H$_4$)}$_2$(4-PPh$_2$py)$_4${Pt(DIOP)}$_2$](CF$_3$SO$_3$)$_6$** (**[1PtaL]$_2$**) in CD_2Cl_2 at 298 K.

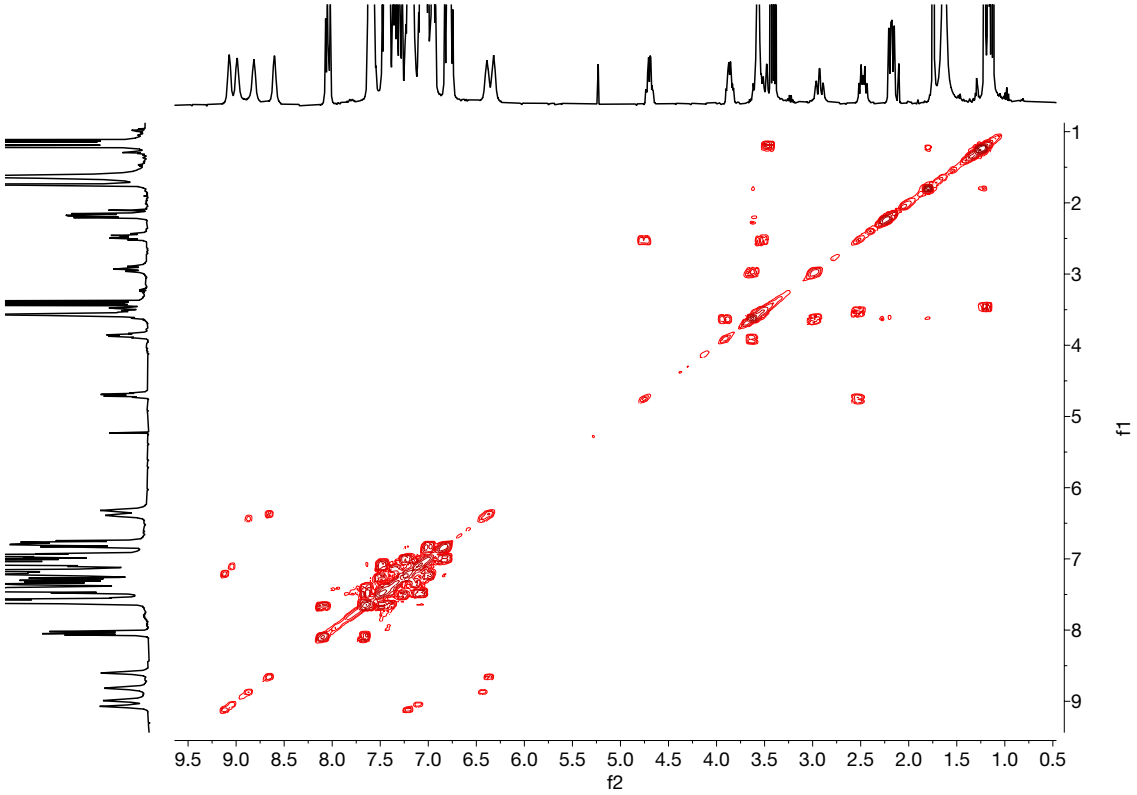

Figure S29. ^{1}H-^{1}H COSY NMR of **[{Pd(η^{3}-2-Me-C$_{3}$H$_{4}$)}$_{2}$(4-PPh$_{2}$py)$_{4}$\{Pt(DIOP)\}$_{2}$](CF$_{3}$SO$_{3}$)$_{6}$ ([1PtaL]$_{2}$)** in $CDCl_3$ at 298 K.

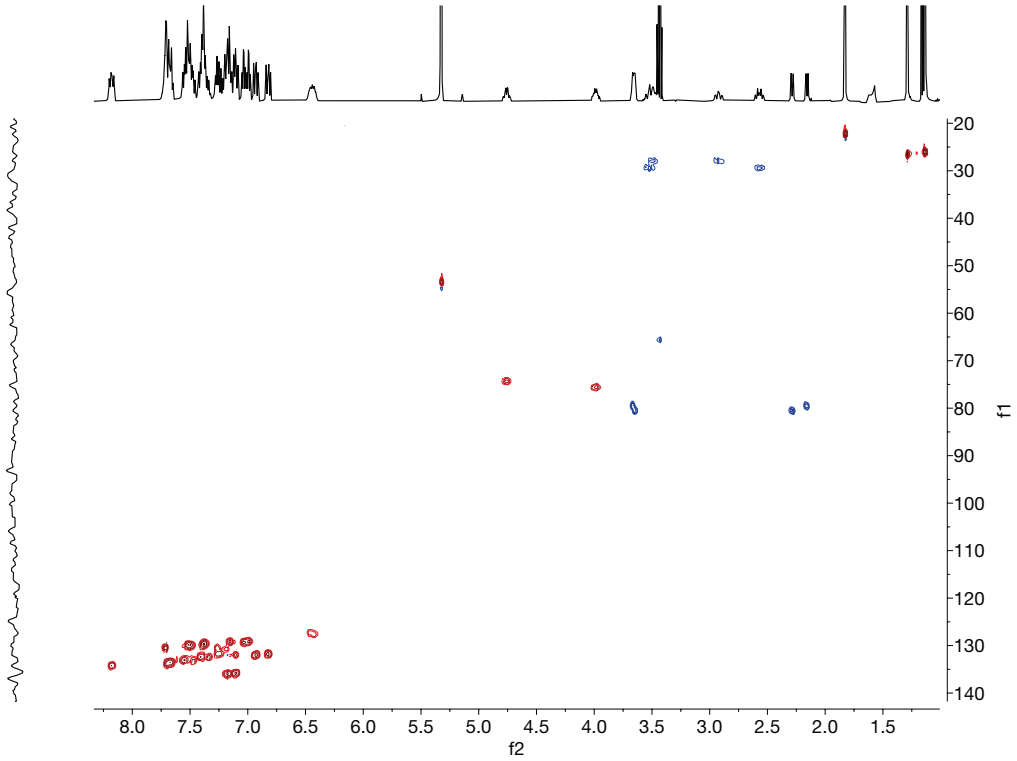

Figure S30. ^{1}H-^{13}C gHSQC NMR of **[{Pd(η^{3}-2-Me-C$_{3}$H$_{4}$)}$_{2}$(4-PPh$_{2}$py)$_{4}$\{Pt(DIOP)\}$_{2}$](CF$_{3}$SO$_{3}$)$_{6}$ ([1PtaL]$_{2}$)** in CD_2Cl_2 at 298 K.

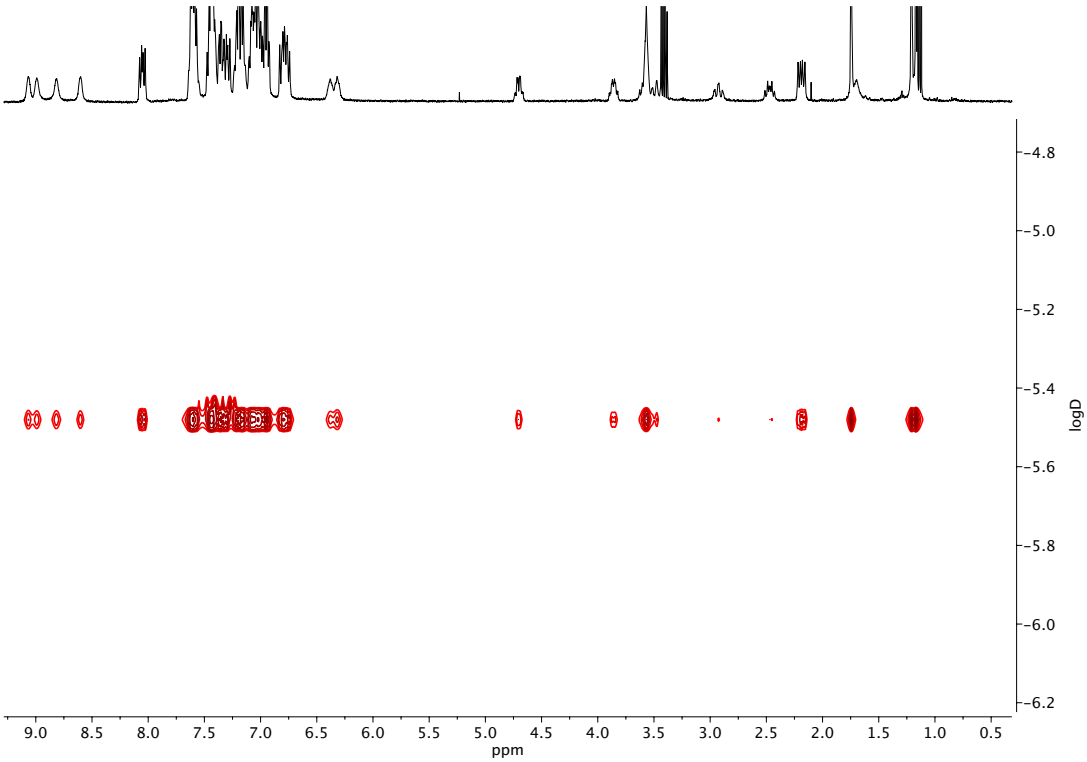

Figure S31. DOSY NMR spectrum of **[{Pd(η^3-2-Me-C$_3$H$_4$)}$_2$(4-PPh$_2$py)$_4$\{Pt(DIOP)\}$_2$](CF$_3$SO$_3$)$_6$ ([1PtaL]$_2$)** in $CDCl_3$ at 298 K.

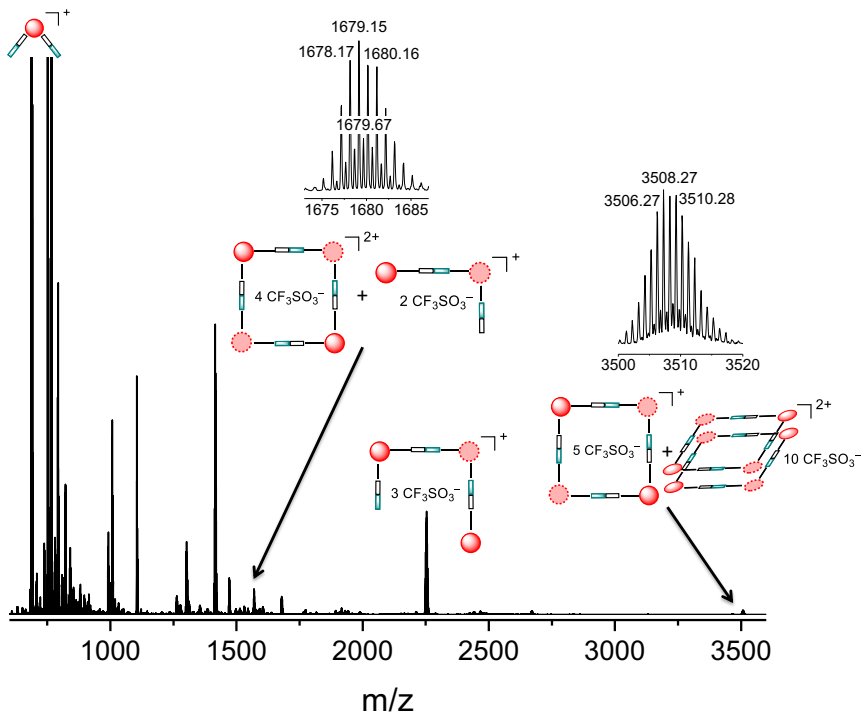

Figure S32. ESI(+)-HRMS spectrum of **[{Pd(η^3-2-Me-C$_3$H$_4$)}$_2$(4-PPh$_2$py)$_4$\{Pt(DIOP)\}$_2$](CF$_3$SO$_3$)$_6$ ([1PtaL]$_2$)**.

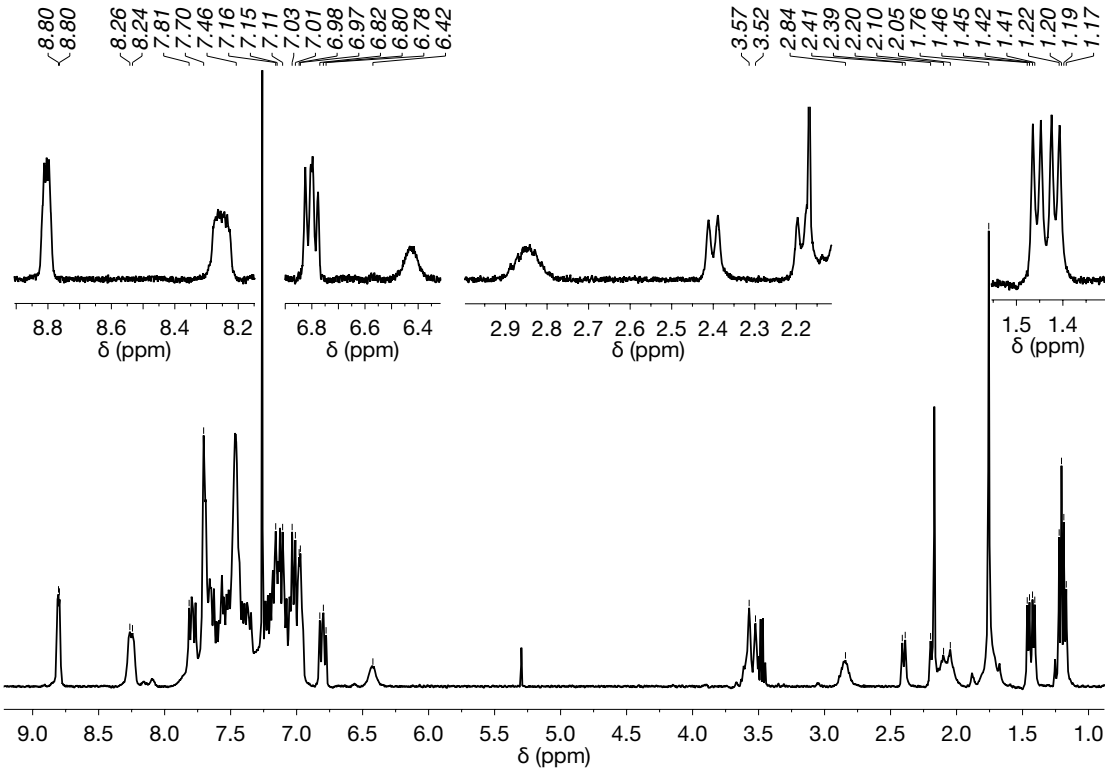

Figure S33. ^{1}H NMR of **[{Pd(η^{3}-2-Me-C$_{3}$H$_{4}$)}$_{2}$(4-PPh$_{2}$py)$_{4}${Pd(BDPP)}$_{2}$](CF$_{3}$SO$_{3}$)$_{6}$** (**[2PdaL]$_{2}$**) in $CDCl_3$ at 298 K.

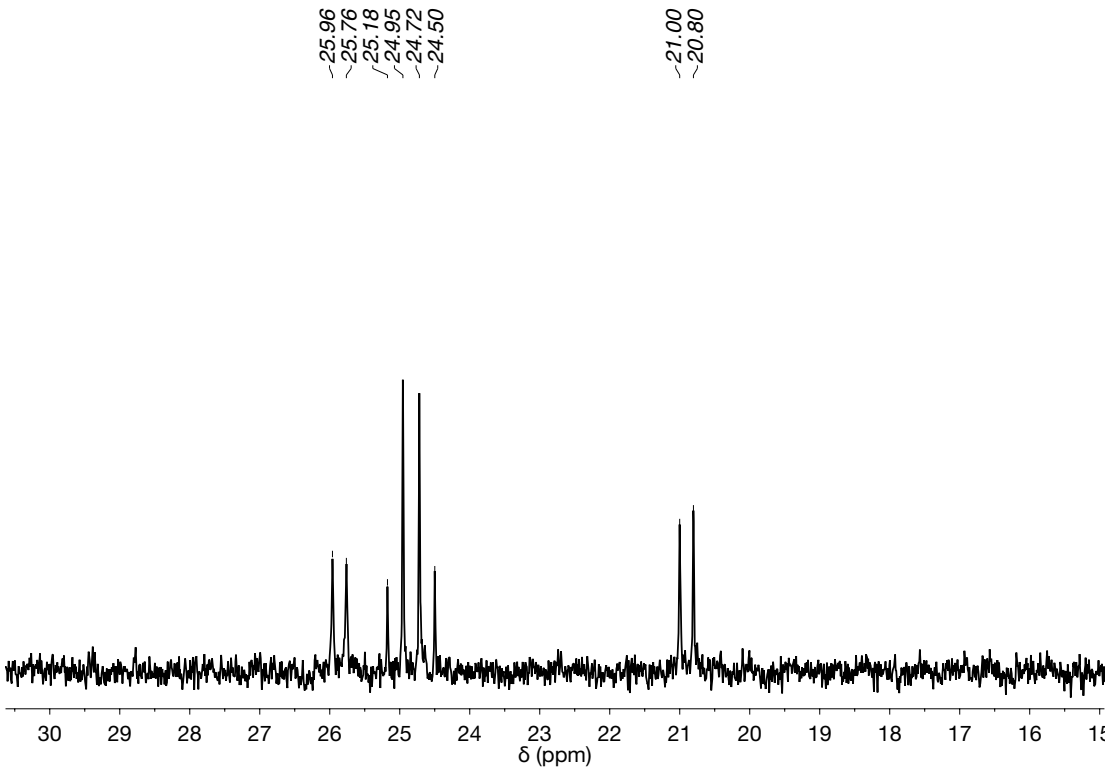

Figure S34. ^{31}P{^{1}H} NMR of **[{Pd(η^{3}-2-Me-C$_{3}$H$_{4}$)}$_{2}$(4-PPh$_{2}$py)$_{4}${Pd(BDPP)}$_{2}$](CF$_{3}$SO$_{3}$)$_{6}$** (**[2PdaL]$_{2}$**) in $CDCl_3$ at 298 K.

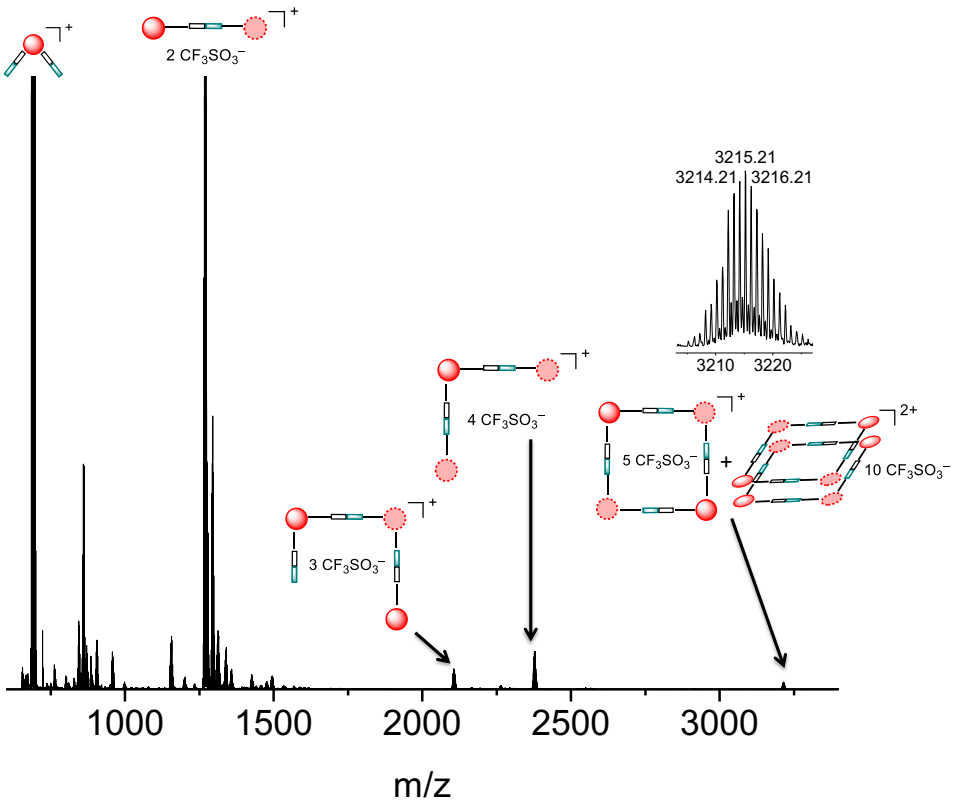

Figure S35. ESI(+)-HRMS spectrum of **[{Pd(η^3-2-Me-C$_3$H$_4$)}$_2$(4-PPh$_2$py)$_4${Pd(BDPP)}$_2$](CF$_3$SO$_3$)$_6$** (**[2PdaL]$_2$**).

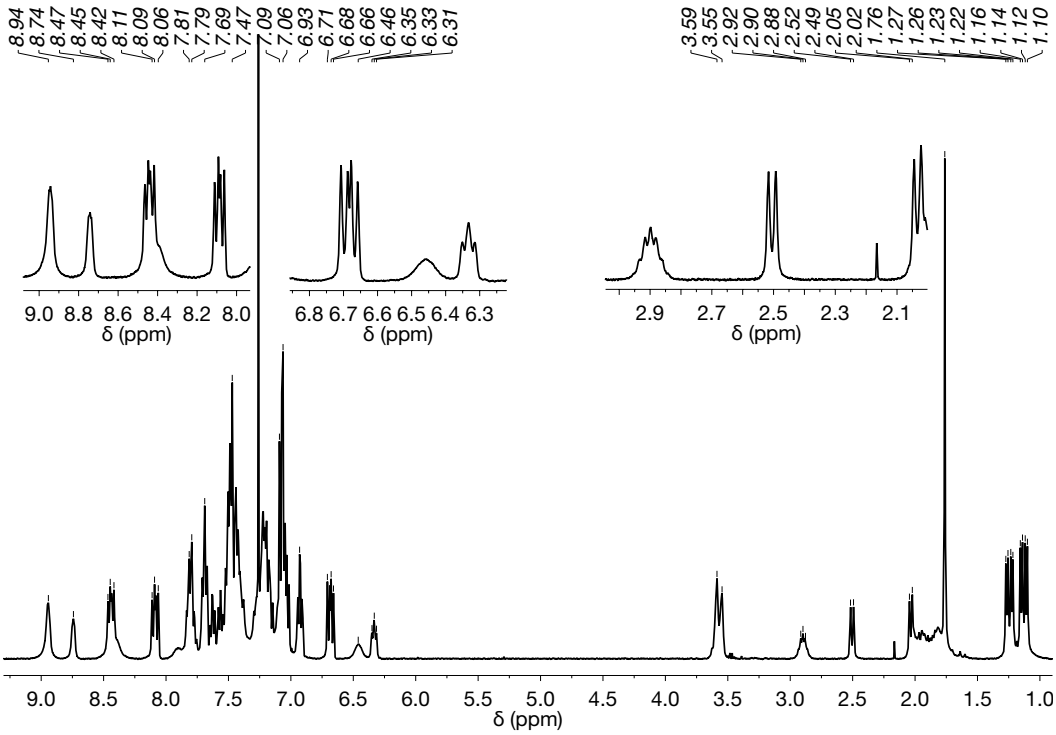

Figure S36. ^{1}H NMR of **[{Pd(η^3-2-Me-C$_3$H$_4$)}$_2$(4-PPh$_2$py)$_4${Pt(BDPP)}$_2$](CF$_3$SO$_3$)$_6$** (**[2PtaL]$_2$**) in CDCl$_3$ at 298 K.

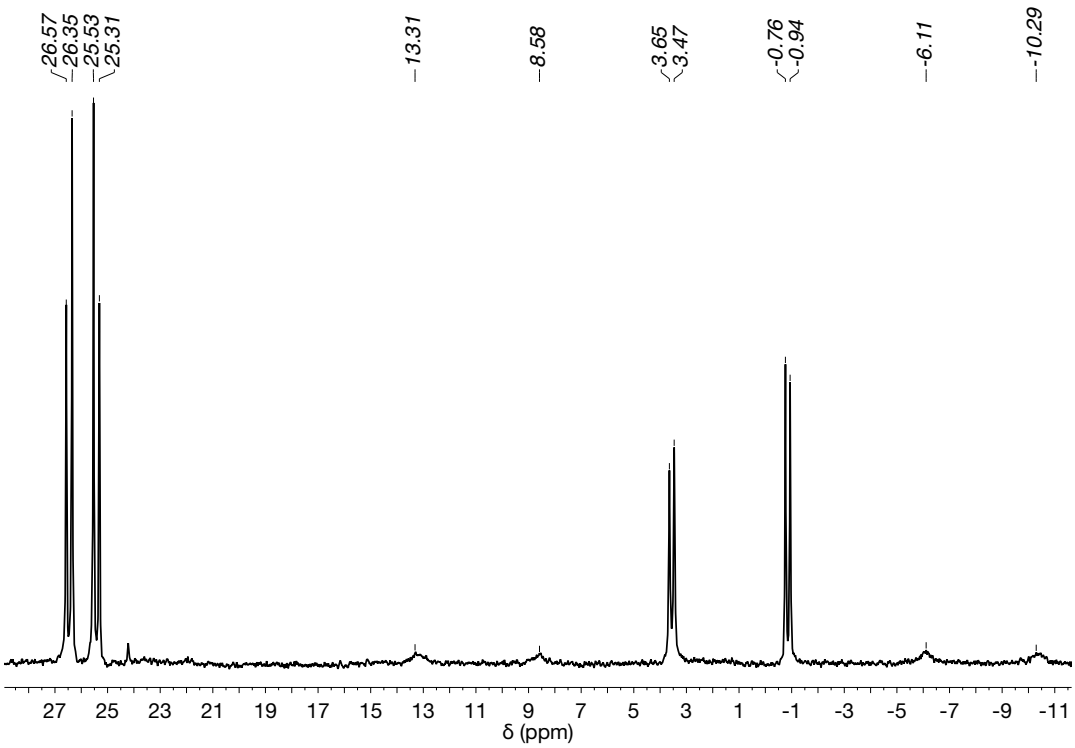

Figure S37. $^{31}P\{^{1}H\}$ NMR of **[{Pd(η^3-2-Me-C$_3$H$_4$)}$_2$(4-PPh$_2$py)$_4${Pt(BDPP)}$_2$](CF$_3$SO$_3$)$_6$ ([2PtaL]$_2$)** in $CDCl_3$ at 298 K.

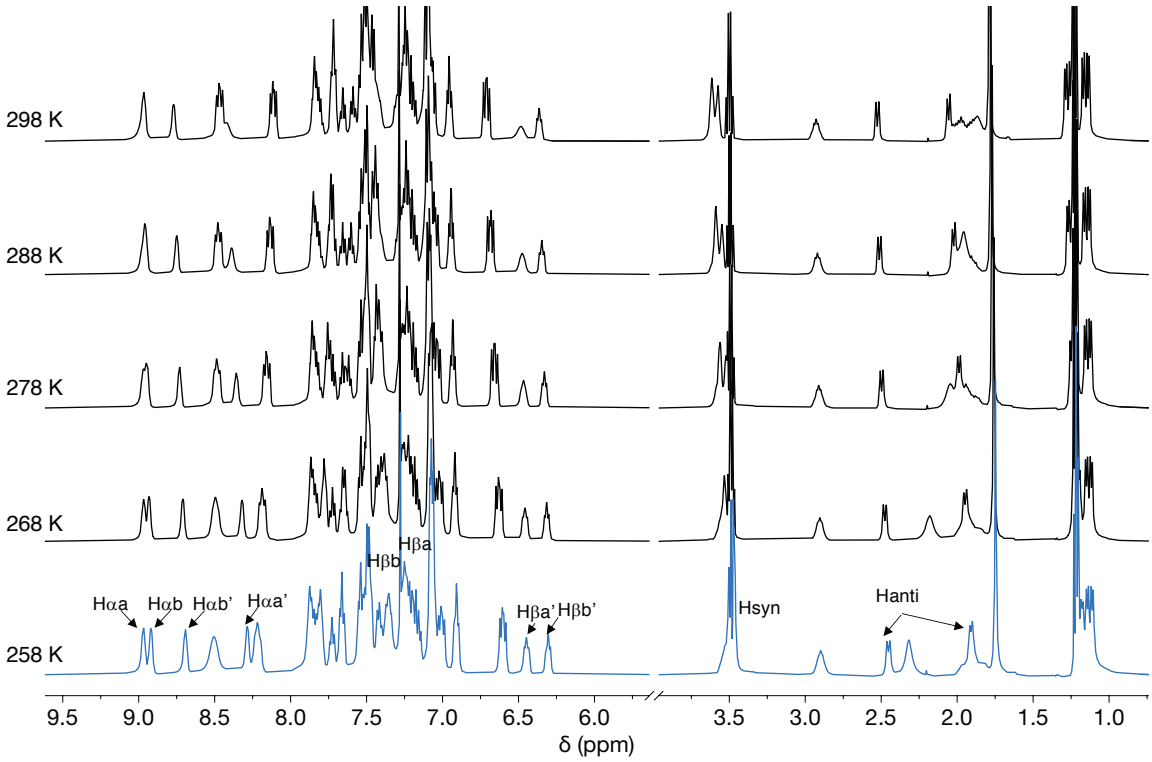

Figure S38. Variable temperature ^{1}H NMR spectra of **[{Pd(η^3-2-Me-C$_3$H$_4$)}$_2$(4-PPh$_2$py)$_4${Pt(BDPP)}$_2$](CF$_3$SO$_3$)$_6$ ([2PtaL]$_2$)** in $CDCl_3$.

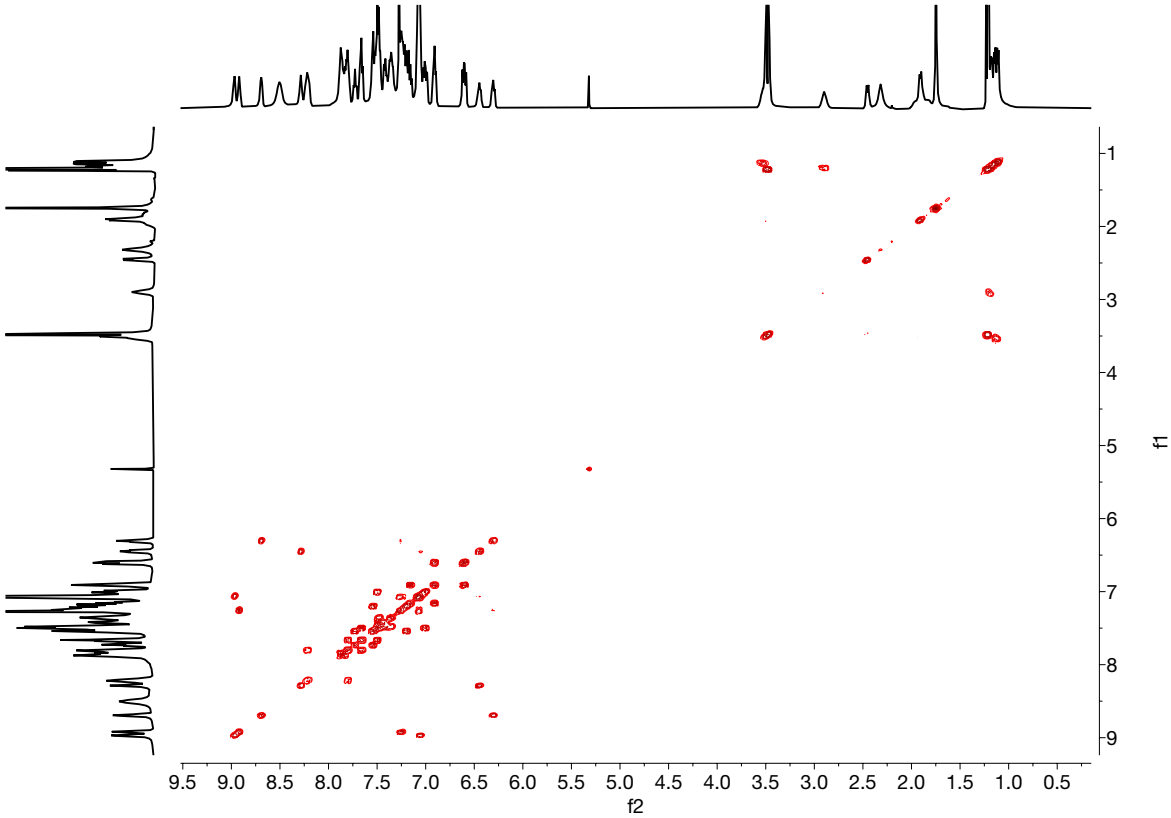

Figure S39. ^{1}H-^{1}H COSY NMR of **[{Pd(η^3-2-Me-C$_3$H$_4$)}$_2$(4-PPh$_2$py)$_4${Pt(BDPP)}$_2$](CF$_3$SO$_3$)$_6$ ([2PtaL]$_2$)** in $CDCl_3$ at 258 K.

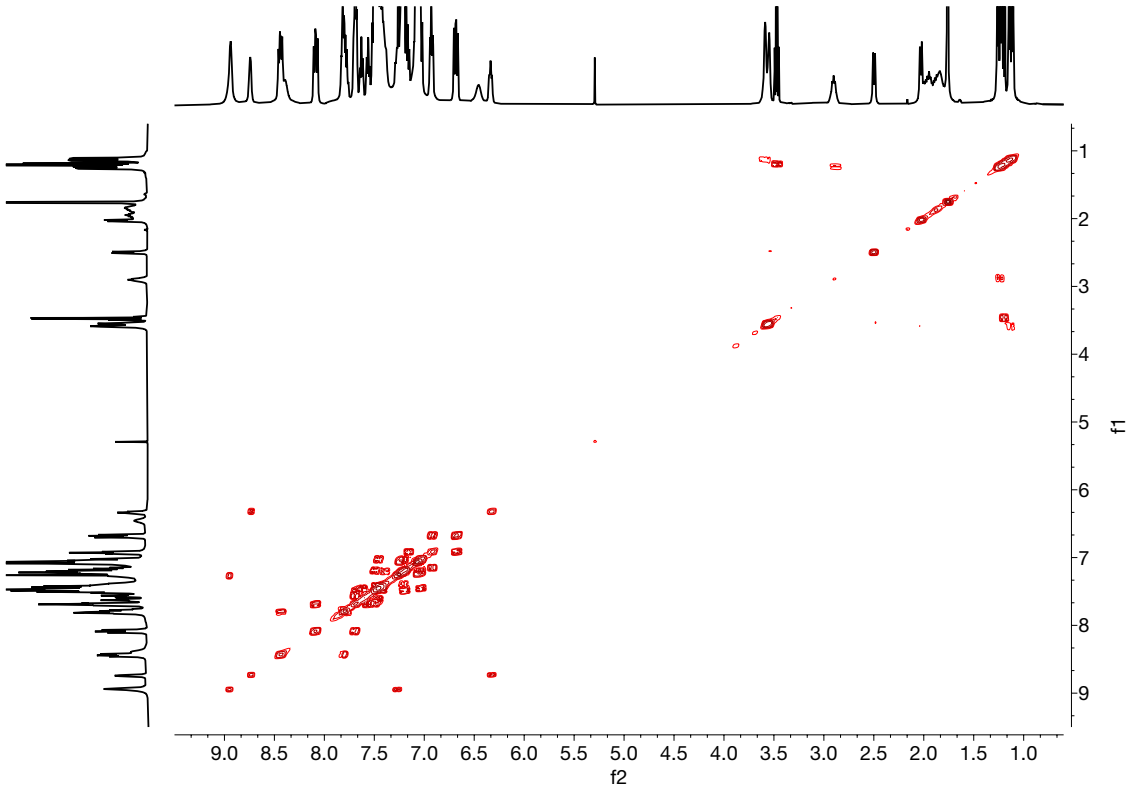

Figure S40. ^{1}H-^{1}H COSY NMR of **[{Pd(η^3-2-Me-C$_3$H$_4$)}$_2$(4-PPh$_2$py)$_4${Pt(BDPP)}$_2$](CF$_3$SO$_3$)$_6$ ([2PtaL]$_2$)** in $CDCl_3$ at 298 K.

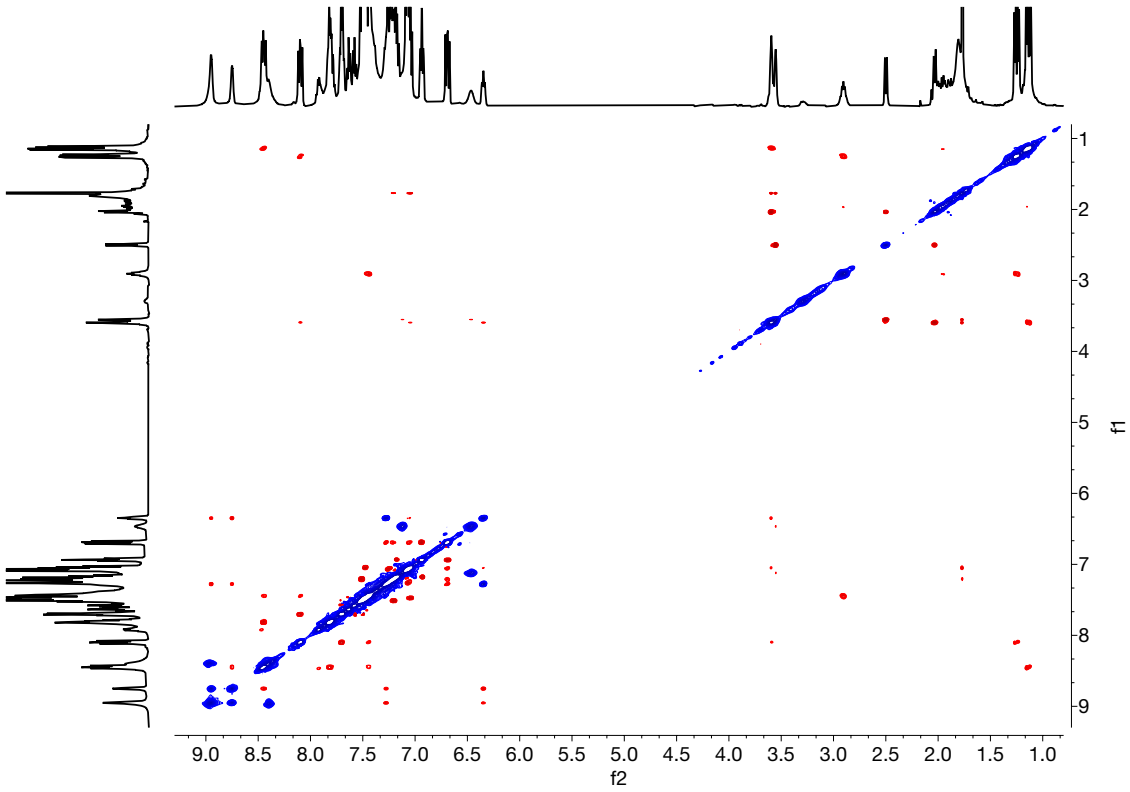

Figure S41. ^{1}H-^{1}H ROESY NMR of **[{Pd(η^{3}-2-Me-C$_{3}$H$_{4}$)}$_{2}$(4-PPh$_{2}$py)$_{4}$\{Pt(BDPP)\}$_{2}$](CF$_{3}$SO$_{3}$)$_{6}$ ([2PtaL]$_{2}$)** in $CDCl_3$ at 298 K.

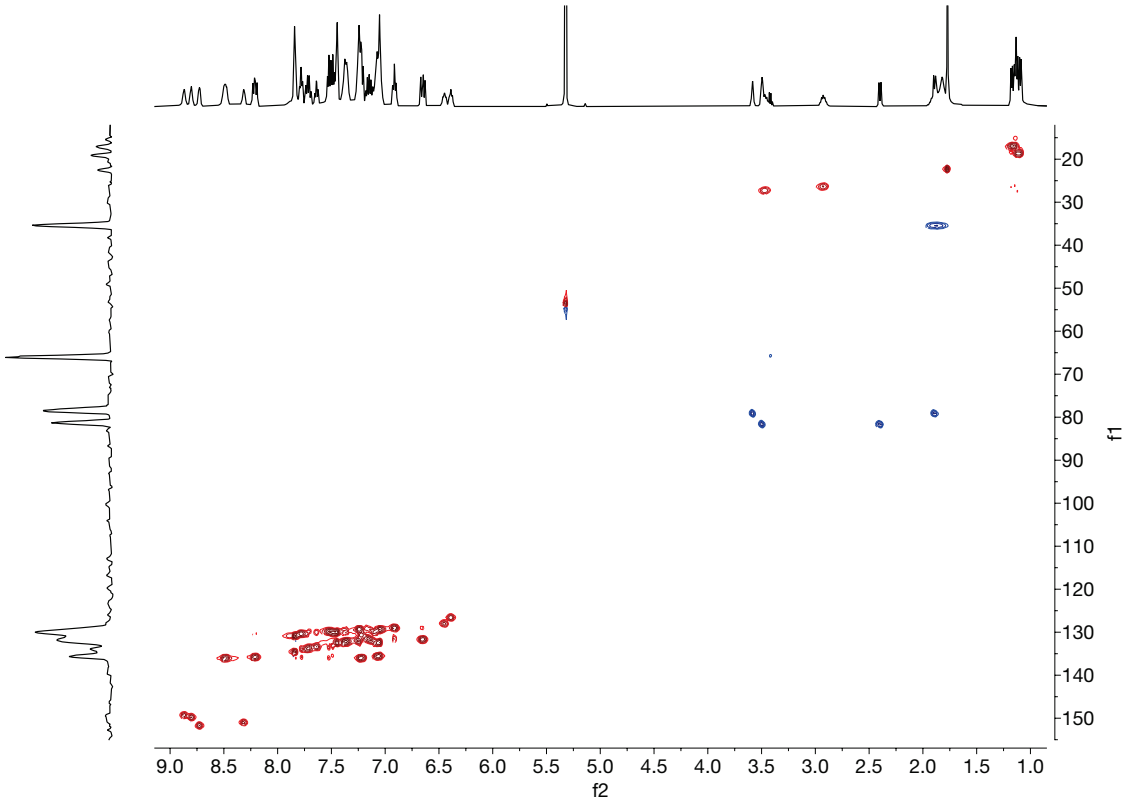

Figure S42. ^{1}H-^{13}C gHSQC NMR of **[{Pd(η^{3}-2-Me-C$_{3}$H$_{4}$)}$_{2}$(4-PPh$_{2}$py)$_{4}$\{Pt(BDPP)\}$_{2}$](CF$_{3}$SO$_{3}$)$_{6}$ ([2PtaL]$_{2}$)** in CD_2Cl_2 at 278 K.

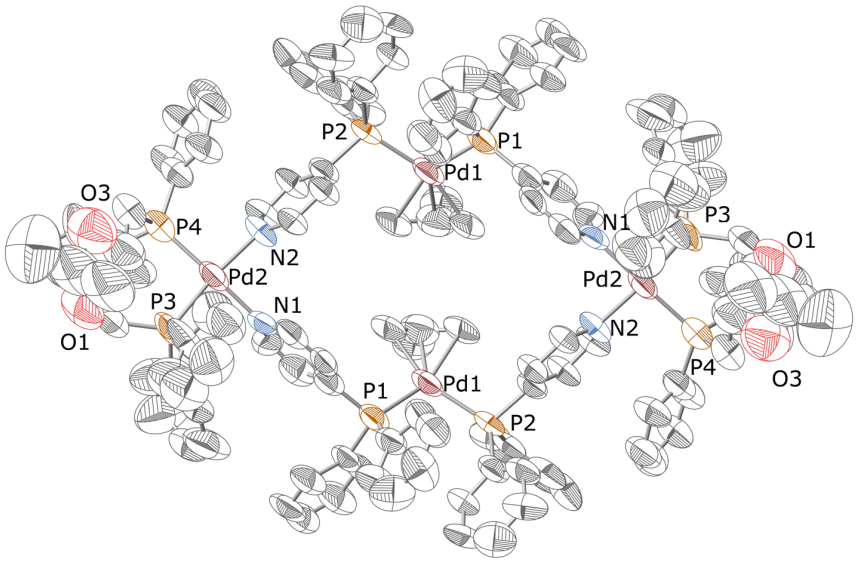

Figure S43. ORTEP plot of **[{Pd(η^3-2-Me-C$_3$H$_4$)}$_2$(4-PPh$_2$py)$_4${Pd(DIOP)}$_2$](CF$_3$SO$_3$)$_6$** (**[1PdaL]$_2$**) with the ellipsoids at 50% probability level. H atoms have been omitted for clarity.

Crystal data for **[1PdaL]$_2$**: CCDC-20006005, $C_{144}H_{134}F_{18}N_4O_{22}P_8Pd_4S_6$, M = 3480.26 g/mol, yellow block, 0.2541 x 0.240 x 0.1434 mm^3, orthorhombic, space group *Fddd*, a = 34.0893(10) Å, b = 39.0572(5) Å, c = 53.629(2) Å, α = 90°, β = 90°, γ = 90°, V = 71403(4) Å^3, Z = 16, D_{calc} = 1.295 g/cm^3, F000 = 28224, μ= 5.177 mm^{-1} , T = 123.00(10) K, θ_{max} = 66.50°, 53165 total reflections, 9243 with Io > 2σ(Io), R_{int} = 0.0520, 15723 data, 889 parameters, 188 restraints, GooF = 1.566, R = 0.1443 and wR= 0.4136 [Io > 2σ(Io)], R = 0.1775 and wR= 0.4559 (all reflections), 2.613 < dΔρ < -1.515 e/Å^3.

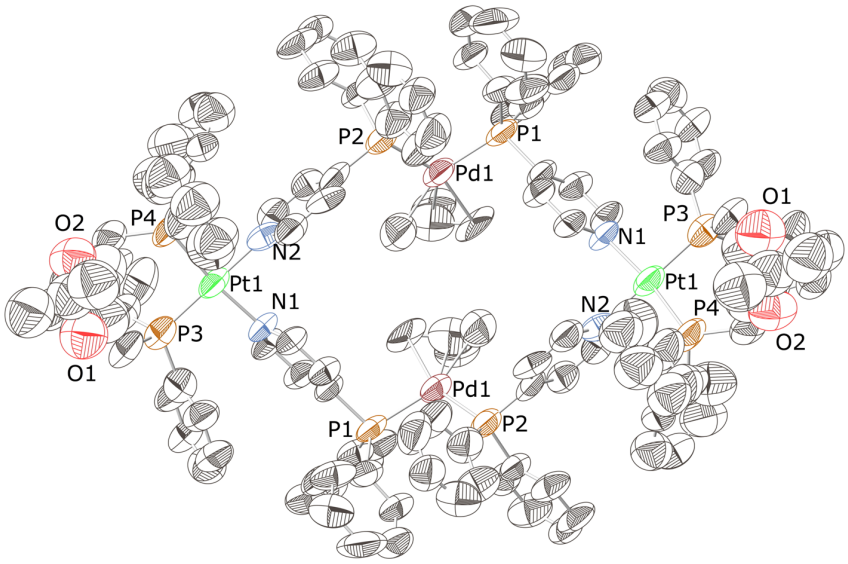

Figure S44. ORTEP plot of **[{Pd(η^3-2-Me-C$_3$H$_4$)}$_2$(4-PPh$_2$py)$_4${Pt(DIOP)}$_2$](CF$_3$SO$_3$)$_6$** (**[1PtaL]$_2$**) with the ellipsoids at 50% probability level. H atoms have been omitted for clarity.

Crystal data for **[1PtaL]$_2$**: CCDC-20006006, $C_{144}H_{134}F_{18}N_4O_{22}P_8Pd_2Pt_2S_6$, M = 3657.64 g/mol, yellow plate, 0.1734 x 0.143 x 0.0778 mm^3, orthorhombic, space group *Fddd*, a = 34.1344(8) Å, b = 39.0265(9) Å, c = 54.2199(15) Å, α = 90°, β = 90°, γ = 90°, V = 72229(3) Å^3, Z = 16, D_{calc} = 1.345 g/cm^3, F000 = 29248, μ= 6.367 mm^{-1} , T = 120.00(10) K, θ_{max} = 66.749 °, 78441 total reflections, 9448 with Io > 2σ(Io), R_{int} = 0.0972, 15943 data, 749 parameters, 259 restraints, GooF = 1.602, R = 0.1537 and wR= 0.4237 [Io > 2σ(Io)], R = 0.1818 and wR= 0.4682 (all reflections), 5.434 < dΔρ < --1.872 e/Å^3.

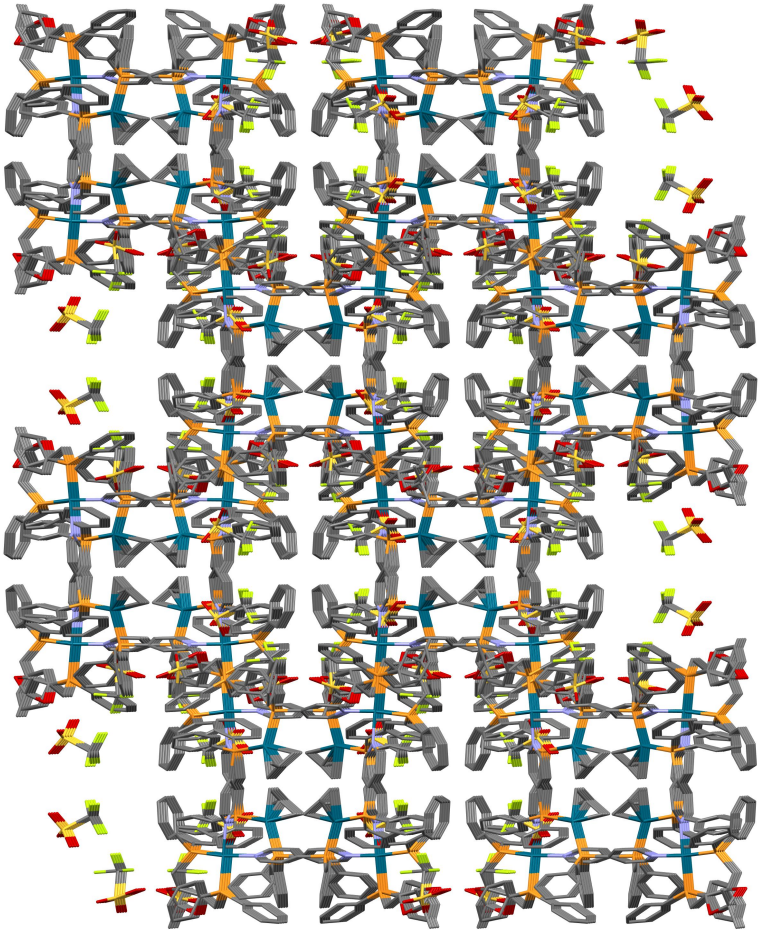

Figure S45. View of the molecular packing of compound **[{Pd(η^3-2-Me-C_3H_4)}$_2$(4-PPh$_2$py)$_4${Pd(DIOP)}$_2$](CF$_3$SO$_3$)$_6$** (**[1PdaL]$_2$**) along the crystallographic *a*-axis

General Procedure for Asymmetric allylic substitution reactions

Pd-catalysed allylic alkylation of rac-(E)-3-acetoxy-1,3-diphenyl-1-propene (S2)

Under a nitrogen atmosphere, the appropriate Pd complex ($0.25 \cdot 10^{-2}$ mmol), substrate *rac*-(*E*)-3-acetoxy-1,3-diphenyl-1-propene, (0.5 mmol) and sodium dimethyl malonate (0.75 mmol) were dissolved in dichloromethane (4 mL) in this precise order. The flask was covered with aluminium foil, and the mixture was stirred for the allotted time. To quench the reaction, diethyl ether (20 mL) and aqueous 10% ammonium chloride solution (20 mL) were added. After extraction, the organic phase was dried with anhydrous sodium sulphate, filtered and the solvent was removed *in vacuo*. The crude product was analysed by ^{1}H NMR spectroscopy to estimate the conversion. Afterwards, the crude product was dissolved in ethyl acetate, and the solution was purified through a column of silica to remove the metallic impurities. The eluent was then removed *in vacuo* and the residue was analysed by NMR spectroscopy and HPLC.[35] In all cases, 10 mg of product were dissolved in 20 mL of the eluent and subsequently filtered before the injection of the sample in the HPLC. The specific conditions are depicted in Table S1.

Pd-catalysed allylic alkylation of rac-1,3-dimethyl-3-acetoxy-1-propene (S3) and rac-3-acetoxycyclohexene (S4)

Under a nitrogen atmosphere, the appropriate Pd complex ($0.25 \cdot 10^{-2}$ mmol), substrate (1 mmol), dimethyl malonate (3 mmol), *N,O*-bis(trimethylsilyl)acetamide (BSA) (3 mmol) and potassium acetate (0.01 mmol) were dissolved in dichloromethane (4 mL) in this precise order. The flask was covered with aluminium foil, and the mixture was stirred for the allotted time. To quench the reaction, diethyl ether (20 mL) and aqueous 10% ammonium chloride solution (20 mL) were added. After extraction, the organic phase was dried with anhydrous sodium sulphate, filtered and the solvent was removed *in vacuo*. The crude product was analysed by ^{1}H NMR spectroscopy to estimate the conversion. Afterwards, the crude product was dissolved in ethyl acetate, and the solution was purified through a column of silica to remove the metallic impurities. The eluent was then removed *in vacuo* and the residue was analysed by NMR spectroscopy and GC. The specific conditions for the GC analysis are depicted in Table S2 and S3.

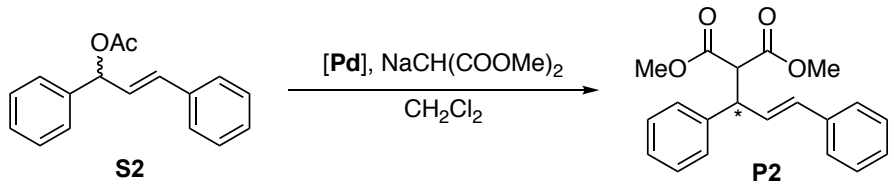

Eluent	95:5 *n*-hexane/*i*PrOH
Flux	0.5 mL/min
Column head pressure	300-350 psi
Temperature programme	25 ºC, 30 min
t_R, (*S*)-**S1**	11.6 min
t_R, (*R*)-**S1**	12.4 min
t_R, (*R*)-**P1**	13.4 min
t_R, (*S*)-**P1**	14.2 min

Table S1. Specific conditions of the HPLC analyses of the asymmetric allylic alkylation of *rac*-(*E*)-3-acetoxy-1,3-diphenyl-1-propene (**S2**).

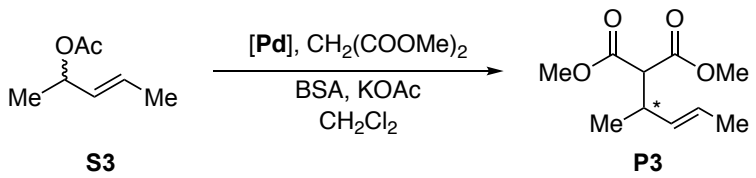

Capillary chiral column	Hydrodex β–3
Flux	80 KPa (H_2)
Temperature programme	60°C (36 min) 60°C→120°C (0.5°C/min) 120°C (20 min)
t_R, (*S*)-**P2**	75.9 min
t_R, (*R*)-**P2**	76.8 min

Table S2. Specific conditions of the GC analyses of the asymmetric allylic alkylation of *rac*-1,3-dimethyl-3-acetoxy-1-propene (**S3**).

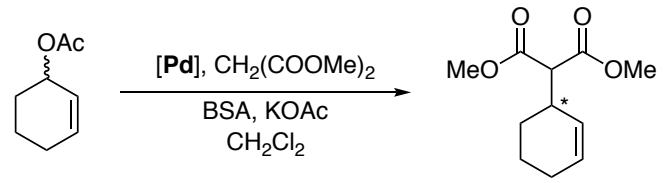

S4 **P4**

Capillary chiral column	Chiraldex B-DM
Flux	90 kPa (He)
Temperature programme	Isotherm at 110°C
t_R, (*S*)-S3	5,7 min
t_R, (*R*)-S3	5,8 min
t_R, (*S*)-P3	26,4 min
t_R, (*R*)-P3	26,8 min

Table S3. Specific conditions of the GC analyses of the asymmetric allylic alkylation of *rac*-3-acetoxycyclohexene (**S4**).